Electronic Supplementary Material (ESI) for ChemComm.

Stackable Molecular Chairs

Han Xie, Lei Zhiquan, Radoslav Z. Pavlović, Judith Gallucci and Jovica D. Badjić*

Department of Chemistry and Biochemistry, The Ohio State University, 100 West 18th Avenue, Columbus, OH 43210

E-mail: badjic.1@osu.edu

SUPPORTING INFORMATION

Table of Contents

General Information

All chemicals were purchased from commercial sources and used as received unless stated otherwise. All solvents were dried prior to use according to standard literature procedures. Chromatographic purifications were performed with silica gel 60 (SiO_2, Sorbent Technologies 40-75 μm, 200 x 400 mesh). Thin-layer chromatography (TLC) was performed on silica-gel plate w/UV254 (200 μm). For NMR studies, we used class B glass NMR tubes (Wilmad Lab Glass). NMR experiments were performed with Bruker 400, 600, 700 and 850 MHz spectrometers. Chemical shifts are expressed in parts per million (δ, ppm) while coupling constant values (J) are given in Hertz (Hz). Residual solvent resonances were used as internal standards: for ^{1}H NMR spectra $CDCl_3$ = 7.26 ppm, $(CD_3)_2SO$ = 2.50 ppm, CD_3OD = 3.31 ppm and D_2O = 4.79 ppm while for ^{13}C NMR spectra $CDCl_3$ = 77.0 ppm, $(CD_3)_2SO$ = 41.23 ppm and CD_3OD = 49.00 ppm. Deuterated solvents CD_3OD, $CDCl_3$, D_2O and $(CD_3)_2SO$ were purchased from Cambridge Isotope Laboratories. HRMS data were obtained on a Bruker-ESI TOF instrument. The calibrations of pH were completed with HI 2210 pH meter.

Synthetic Procedures

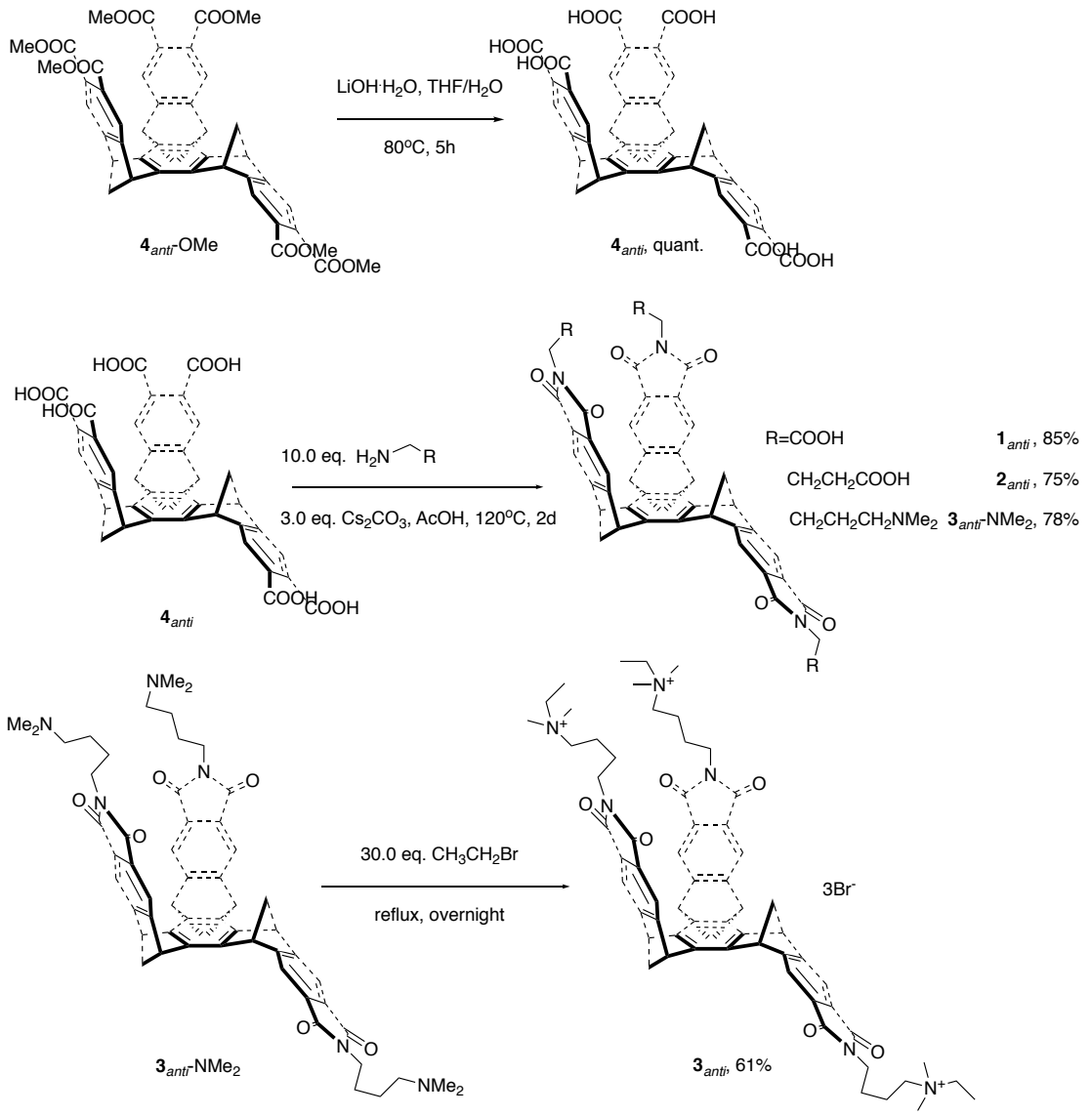

Scheme S1. Synthetic scheme describing the preparation of **1**–**3**$_{anti}$ from **4**$_{anti}$. (Top) Compound **4**$_{anti}$ was obtained by base-promoted hydrolysis from hexaester **4**$_{anti}$–OMe (for preparing this compound, see: Border, S. E.; Pavlovic, R. Z.; Lei, Z. Q.; Badjic, J. D., *J. Am. Chem. Soc.* **2017,** *139*, 18496-18499). (Bottom) For obtaining **3**$_{anti}$, we alkylated the condensation product **3**$_{anti}$–NMe_2 with ethyl bromide.

Compound $\mathbf{4}_{anti}$: Hexaester $\mathbf{4}_{anti}$–OMe (252 mg, 0.328 mmol) and LiOH · H_2O (421 mg, 9.8 mmol) were dissolved in 1:1 THF/H_2O (30 mL) and the solution was brought to 80 °C for 5h; for obtaining $\mathbf{4}_{anti}$–OMe, see: Border, S. E.; Pavlovic, R. Z.; Lei, Z. Q.; Badjic, J. D., *J. Am. Chem. Soc.* **2017,** *139*, 18496-18499. After cooling down the reaction mixture to room temperature, THF was removed under reduced pressure. To the remaining solvent, 10 mL of deionized water was added to dilute the mixture and 1 mL of 0.5 M HCl was added to cause the formation of white precipitate. After centrifugation, decantation and washing of the precipitate with diluted HCl (pH = 3), the remaining wet solid was lyophilized to give $\mathbf{4}_{anti}$ as a white powder in practically quantitative yield (220 mg). ^{1}H NMR (850 MHz, CD_3SOCD_3): δ (ppm) = 12.85 (broad, COOH), 7.63 (s, 2H), 7.57 (s, 2H), 7.54 (s, 2H), 4.61 (s, 2H), 4.61 (s, 2H), 4.59 (s, 2H), 2.39-2.24 (AB quartet, 4H, J = 7.9 Hz), 2.35-2.06 (AB quartet, 2H, J = 7.1 Hz). ^{13}C NMR (213 MHz, CD_3SOCD_3): δ (ppm) = 169.29, 169.15, 169.00, 153.56, 153.42, 153.38, 138.66, 138.49, 138.38, 130.92, 130.77, 130.44, 121.80, 121.71, 121.53, 65.25, 65.14, 48.36, 48.28, 48.25. HRMS (ESI): m/z calcd for $C_{39}H_{23}O_{12}^-$ $[M–H]^-$: 683.1195; found: 683.1229

Compounds $\mathbf{1}_{anti}$/$\mathbf{2}_{anti}$: A solution of $\mathbf{4}_{anti}$ (10 mg, 0.015 mmol), Cs_2CO_3 (49 mg, 0.15 mmol) and amino acids **5** or **6** (12 or 17 mg, 0.16 mmol) in 1 mL of glacial acetic acid was stirred at 120 °C for 2d. After cooling the reaction mixture to room temperature, the solvent was removed under reduced pressure. The solid residue was rinsed with 3 x 5 mL of diluted HCl (pH = 3) to give $\mathbf{1}_{anti}$ or $\mathbf{2}_{anti}$ as an off-white powder after the lyophilization. $\mathbf{1}_{anti}$ was recrystallized from CH_3OH:CH_2Cl_2 = 1:5 after vapor diffusion of Et_2O (10.2 mg, 85% yield). $\mathbf{2}_{anti}$ was recrystallized from CH_2Cl_2 after vapor diffusion of hexanes (10.3 mg, 75% yield). **Compound $\mathbf{1}_{anti}$** : ^{1}H NMR (700 MHz, CD_3SOCD_3): δ (ppm) = 13.15 (broad, COOH), 7.93 (s, 2H), 7.90 (s, 2H), 7.81 (s, 2H), 4.76 (s, 2H), 4.75 (s, 2H), 4.71 (s, 2H), 4.27 (s, 2H), 4.20 (s, 4H), 2.48-2.35 (AB quartet, 4H, J = 8.3 Hz), 2.46-2.15 (AB quartet, 2H, J = 8.4 Hz). ^{13}C NMR (175 MHz, CD_3SOCD_3): δ (ppm) = 169.42, 169.34, 167.89, 167.80, 167.74, 158.68, 158.61, 158.50, 138.76, 138.64, 138.42, 130.21, 130.15, 117.03, 116.95, 116.90, 65.56, 65.19, 48.80, 48.68, 48.66, 39.31, 39.20. HRMS (ESI): m/z calcd for $C_{45}H_{26}N_3O_{12}$ $[M–H]^-$: 800.1516, found: 800.1538. **Compound $\mathbf{2}_{anti}$**: ^{1}H NMR (400 MHz, CD_3SOCD_3): δ (ppm) 12.00 (broad, COOH), 7.85 (s, 2H), 7.82 (s, 2H), 7.74 (s, 2H), 4.74 (s, 2H), 4.73 (s, 2H), 4.69 (s, 2H), 3.58-3.55 (t, 2H, J = 6.6 Hz), 3.51-3.47 (t, 4H, J = 6.8 Hz), 2.48-2.29 (AB quartet, 4H, J = 8.3 Hz), 2.45-2.07 (AB quartet, 2H, J = 8.4 Hz), 2.24-

2.19 (m, 6H), 1.78-1.71 (m, 6H). ^{13}C NMR (175 MHz, CD_3SOCD_3): δ (ppm) = 174.31, 174.27, 168.58, 168.48, 158.04, 157.94, 138.72, 138.60, 138.42, 130.40, 130.36, 130.29, 116.69, 116.58, 65.57, 65.21, 48.77, 48.61, 48.58, 37.26, 37.18, 31.39, 31.33, 23.86, 23.84. HRMS (ESI): *m/z* calcd for $C_{51}H_{39}N_3NaO_{12}$ $[M+Na]^+$: 908.2431; found: 908.2457

Compound 3$_{anti}$**–NMe$_2$**: A solution of **4**$_{anti}$ (20 mg, 0.029 mmol), Cs_2CO_3 (98 mg, 0.29 mmol), *N*',*N*'-dimethylbutane-1,4-diamine **7** (34 mg, 0.29 mmol) in 1 mL glacial acetic acid was stirred at 120 °C for 2d. After cooling the reaction mixture to room temperature, the solvent was removed under reduced pressure. The solid residue was dissolved in 5 mL of water after which 0.1M HCl was added to adjust pH to 3. The aqueous layer was washed with ethyl acetate (3 x 4 mL), followed by changing its pH to 8 with saturated $NaHCO_3$. After the product was extracted with CH_2Cl_2 (5 x 4 mL), the organic layer was dried over Na_2SO_4 and the solvent was removed under vacuum to give **3**$_{anti}$**–NMe$_2$** as a yellow oil (21 mg, 78%). ^{1}H NMR (700 MHz, $CDCl_3$): δ (ppm) = 7.73 (s, 2H), 7.65 (s, 2H), 7.62 (s, 2H), 4.50 (s, 2H), 4.46 (s, 2H), 4.45 (s, 2H), 3.66-3.64 (t, 2H, *J* = 7.1 Hz), 3.59-3.57 (t, 4H, *J* = 7.2 Hz), 2.57-2.41 (AB quartet, 4H, *J* = 8.5 Hz) 2.54-2.28 (AB quartet, 2H, *J* = 8.6 Hz), 2.32-2.24 (m, 6H), 2.21 (s, 6H), 2.18 (s, 12H), 1.67-1.57 (m, 6H), 1.50-1.42 (m, 6H). ^{13}C NMR (175 MHz, $CDCl_3$): δ (ppm) = 168.84, 168.78, 168.46, 157.23, 157.01, 156.86, 138.43, 138.20, 138.16, 130.80, 130.75, 130.73, 116.54, 116.39, 116.37, 65.76, 65.08, 59.21, 59.15, 49.31, 49.12, 45.44, 45.41, 37.82, 37.75, 26.67, 26.64, 24.95, 24.88. HRMS (ESI): *m*/*z* calcd for $C_{57}H_{62}N_6O_{62}^+$ $[M+2H]^{2+}$: 463.2360; found: 463.2355.

Compound 3$_{anti}$: To 3 mL of dry acetonitrile, **3**$_{anti}$**–NMe$_2$** (21 mg, 0.023 mmol) and bromoethane (75 mg, 0.68 mmol) were added and the reaction mixture was brought to reflux overnight. Following, the mixture was cooled to room temperature and the solvent removed under reduced pressure to give a solid product. Recrystallization from CH_3OH : ethyl acetate = 3:1 gave 14 mg of **3**$_{anti}$ as yellow needles (61%). ^{1}H NMR (600 MHz, CD_3OD): δ (ppm) = 7.82 (s, 2H), 7.76 (s, 2H), 7.72 (s, 2H), 4.68 (s, 2H), 4.67 (s, 2H), 4.65 (s, 2H), 3.73-3.71 (t, 2H, *J* = 6.4 Hz), 3.67-3.65 (t, 4H, *J* = 6.5 Hz), 3.42-3.37 (m, 12H), 3.07 (s, 6H), 3.05 (s, 12H), 2.52-2.31 (AB quartet, 4H, *J* = 8.4 Hz) 2.45-2.09 (AB quartet, 2H, *J* = 8.5 Hz), 1.77-1.70 (m, 12H), 1.39-1.35 (m, 9H). ^{13}C NMR (150 MHz, CD_3OD): δ (ppm) = 168.82, 168.76, 168.72, 158.00, 157.98, 157.74, 138.56, 138.32, 138.28, 130.33, 130.29, 130.24, 116.02, 115.96, 115.73, 65.16, 64.61, 62.85, 62.80,

59.66, 49.36, 49.34, 48.86, 48.76, 36.25, 36.22, 25.11, 19.34, 7.10, 7.08. HRMS (ESI): *m/z* calcd for $C_{63}H_{75}N_6O_6$: 337.1911; $[M]^{3+}$, found: 337.1926.

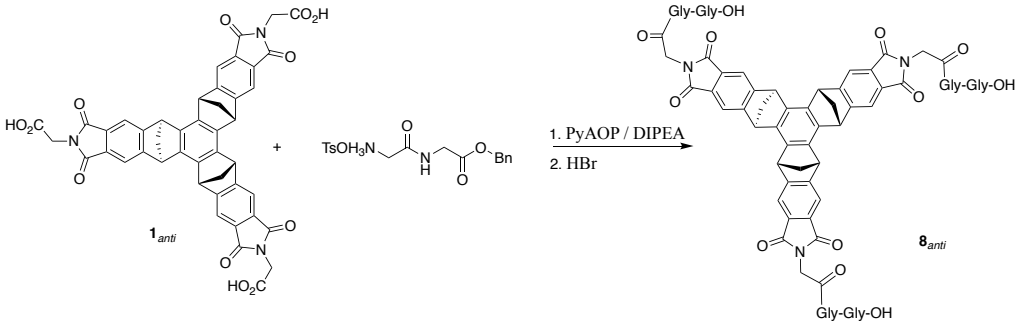

Compound $\mathbf{8}_{anti}$:. To a solution of $\mathbf{1}_{anti}$ (15 mg, 0.019 mmol) in 2 mL of dry DMF, *p*-TsOH Gly-Gly-OBn (28.2 mg, 0.074 mmol), PYAOP (7-Azabenzotriazol-1-yloxy)tripyrrolidinophosphonium hexafluorophosphate; 38.7 mg, 0.074 mmol) and DIPEA (*N*,*N*-diisopropylethylamine; 29.7 uL, 0.17 mmol) were added in one portion. The reaction mixture was stirred overnight. Following, the solvent was removed by a steady nitrogen flow. The crude product was purified by column chromatography (SiO_2; CH_2Cl_2 : CH_3OH = 20:1), to give $\mathbf{8}_{anti}$–OBn as a white powder (24.3 mg, 92%). ^{1}H NMR (850 MHz, CD_3SOCD_3): δ (ppm) = 8.54-8.53 (t, 1H, J = 5.8 Hz), 8.49-8.48 (t, 2H, J = 5.8 Hz). 8.37-8.36 (t, 1H, J = 5.9 Hz), 8.34-8.32 (t, 2H, J = 5.9 Hz), 7.90 (s, 2H), 7.86 (s, 2H), 7.77 (s, 2H), 7.73-7.30 (m, 15H), 5.13 (s, 2H), 5.12 (s, 4H), 4.76 (s, 2H), 4.74 (s, 2H), 4.70 (s, 2H), 4.23 (s, 2H), 4.16 (s, 4H), 3.92-3.91 (d, 2H, J = 5.9 Hz), 3.91-3.90 (d, 4H, J = 5.9 Hz), 3.77-3.76 (d, 2H, J = 5.7 Hz), 3.74-3.73 (d, 4H, J = 5.7 Hz), 2.48-2.33 (AB quartet, 4H, J = 7.5 Hz), 2.46-2.12 (AB quartet, 2H, J = 7.7 Hz). ^{13}C NMR (213 MHz, CD_3SOCD_3): δ (ppm) = 170.09, 170.08, 169.60, 169.59, 168.16, 168.05, 168.03, 167.02, 166.98, 158.38, 158.30, 158.23, 138.72, 138.61, 138.41, 136.34, 136.33, 130.51, 130.46, 130.36, 128.89, 128.88, 128.51, 128.37, 116.85, 116.78, 116.73, 66.31, 65.61, 65.15, 48.81, 48.65, 48.63, 46.34, 46.32, 42.18, 41.13. Compound $\mathbf{8}_{anti}$-OBn (13.6 mg, 0.01 mmol) was dissolved in 1 mL of HBr (33 wt% in CH_3CO_2H) solution. The mixture was brought to 50 °C for 6 h. Following, the solvent was removed under reduced pressure and the solid residue washed by 0.1M HCl solution (2 x 5 mL). The solid was lyophilized to give $\mathbf{8}_{anti}$ as white powder (6 mg, 55%). ^{1}H NMR (700 MHz, CD_3SOCD_3): δ (ppm) = 12.57 (broad, COOH) 8.51-8.50 (t, 1H, J = 5.7 Hz), 8.47-8.45 (t, 2H, J = 5.7 Hz). 8.22-8.20 (t, 1H, J = 5.9 Hz), 8.18-8.17 (t, 2H, J = 5.8 Hz), 7.90 (s, 2H), 7.86 (s, 2H), 7.77 (s, 2H), 4.76 (s, 2H), 4.74 (s, 2H), 4.70 (s, 2H), 4.23 (s, 2H), 4.16 (s, 4H), 3.92-3.91 (d, 2H, J = 5.9 Hz), 3.91-3.90 (d, 4H, J = 5.9 Hz), 3.77-3.72 (m, 12H), 2.49-2.33 (AB quartet, 4H, J

= 7.7 Hz), 2.46-2.13 (AB quartet, 2H, J = 7.7 Hz). ^{13}C NMR (150 MHz, CD_3SOCD_3): δ (ppm) = 171.55, 169.35, 168.18, 168.07, 168.04, 166.99, 166.97, 158.40, 158.33, 158.25, 138.73, 138.62, 138.42, 130.51, 130.46, 130.37, 116.86, 116.79, 116.75, 65.61, 65.16, 48.81, 48.63, 42.20, 41.02. HRMS (ESI): *m/z* Calcd for $C_{57}H_{43}N_9O_{18}^{2-}$: 570.6369; $[M]^{2-}$; found: 570.6363.

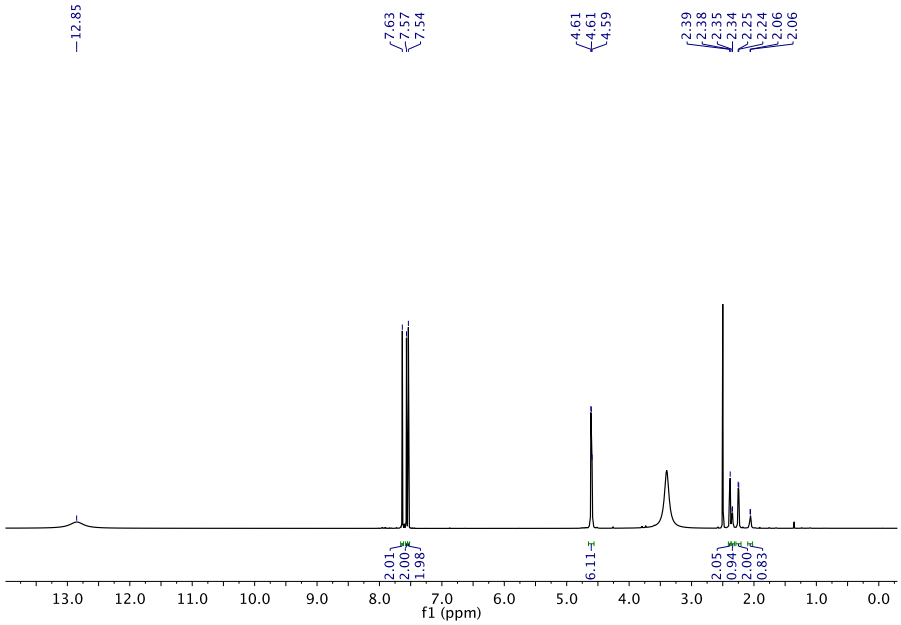

Figure S1. ^{1}H NMR spectrum (850 MHz, 298 K) of $\mathbf{4}_{anti}$ in $(CD_3)_2SO$.

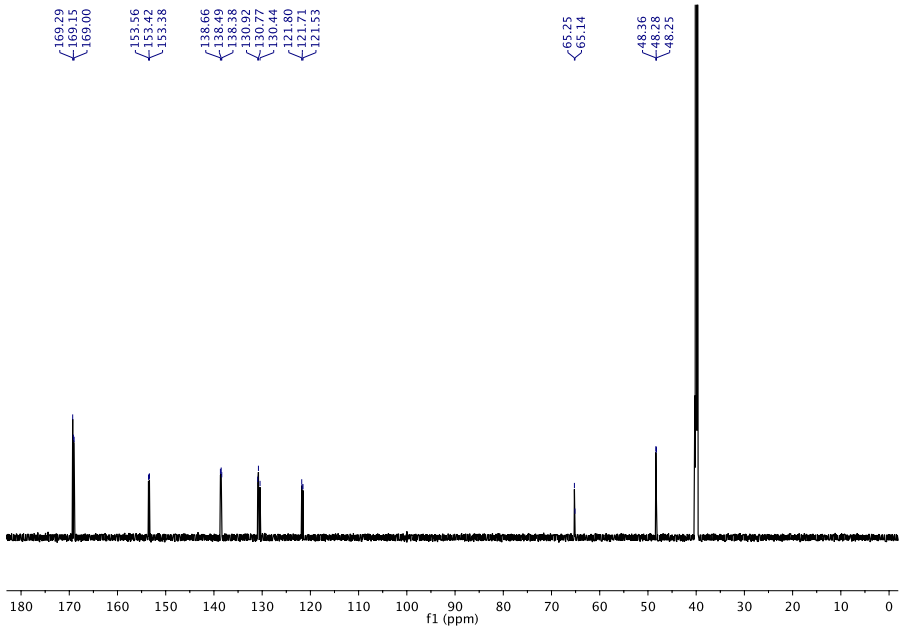

Figure S2. ^{13}C NMR spectrum (213 MHz, 298 K) of $\mathbf{4}_{anti}$ in $(CD_3)_2SO$.

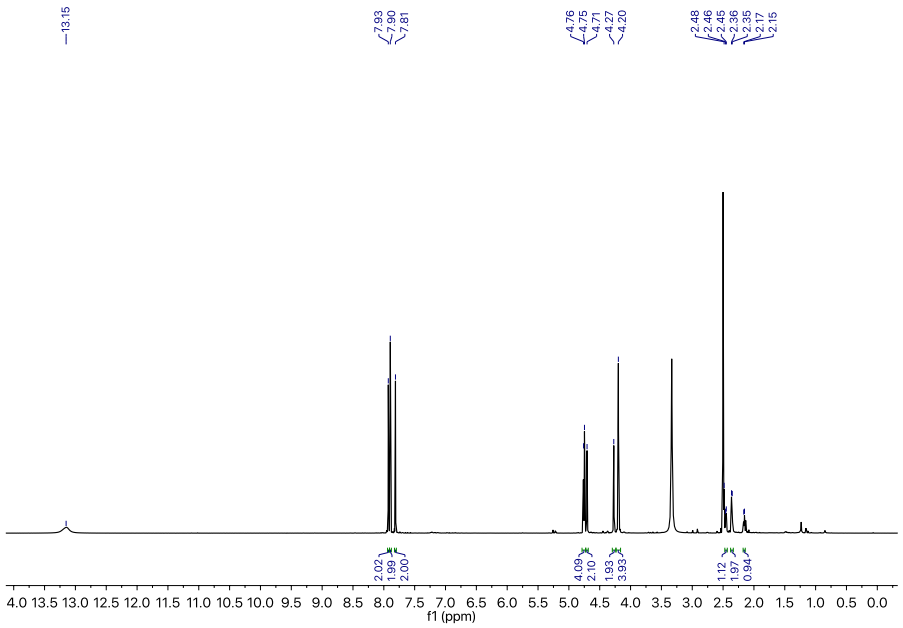

Figure S3. ^{1}H NMR spectrum (700 MHz, 298 K) of 5 mM $\mathbf{1}_{anti}$ in $(CD_3)_2SO$.

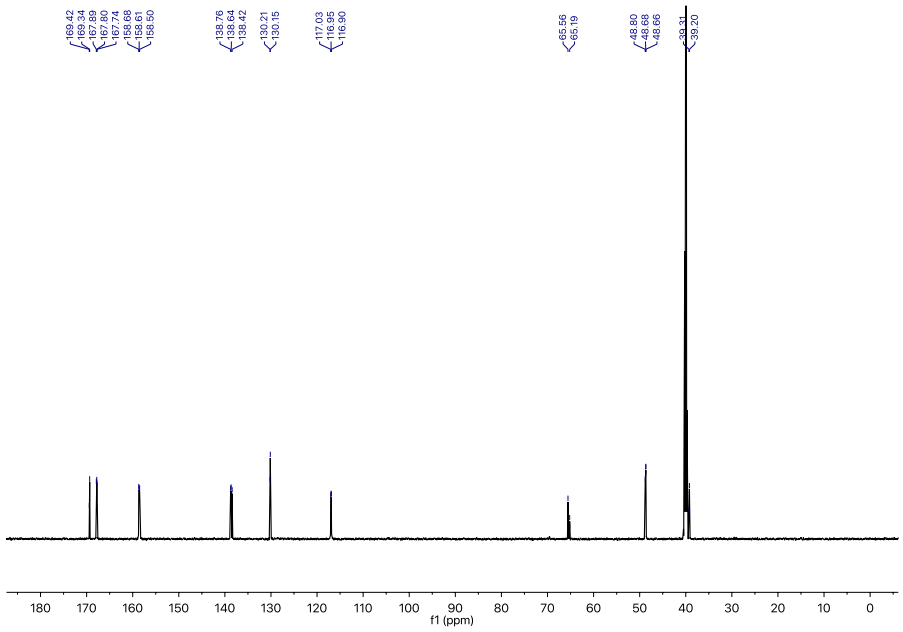

Figure S4. ^{13}C NMR spectrum (175 MHz, 298 K) of 5 mM $\mathbf{1}_{anti}$ in $(CD_3)_2SO$.

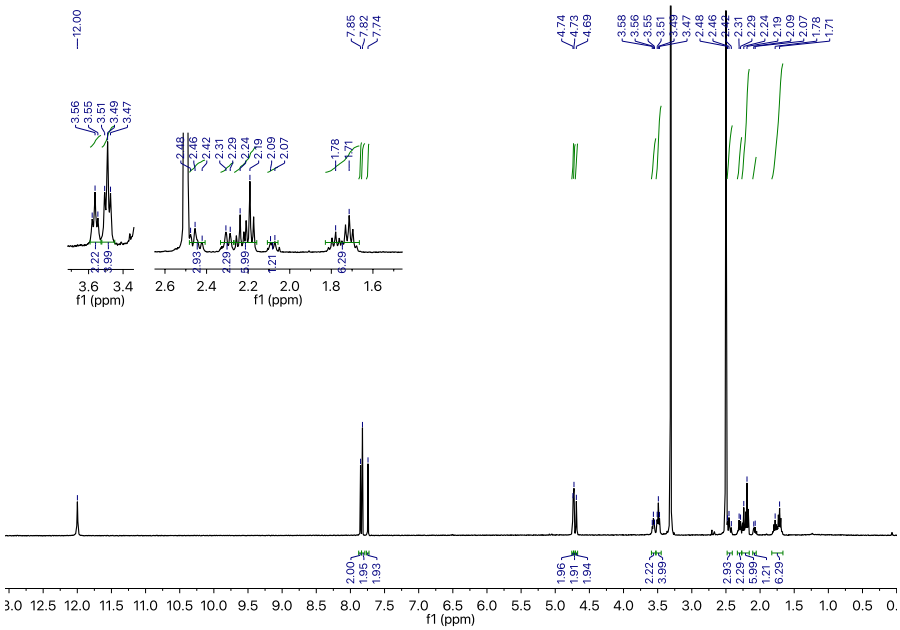

Figure S5. ^{1}H NMR spectrum (400 MHz, 298 K) of 2 mM $\mathbf{2}_{anti}$ in $(CD_3)_2SO$.

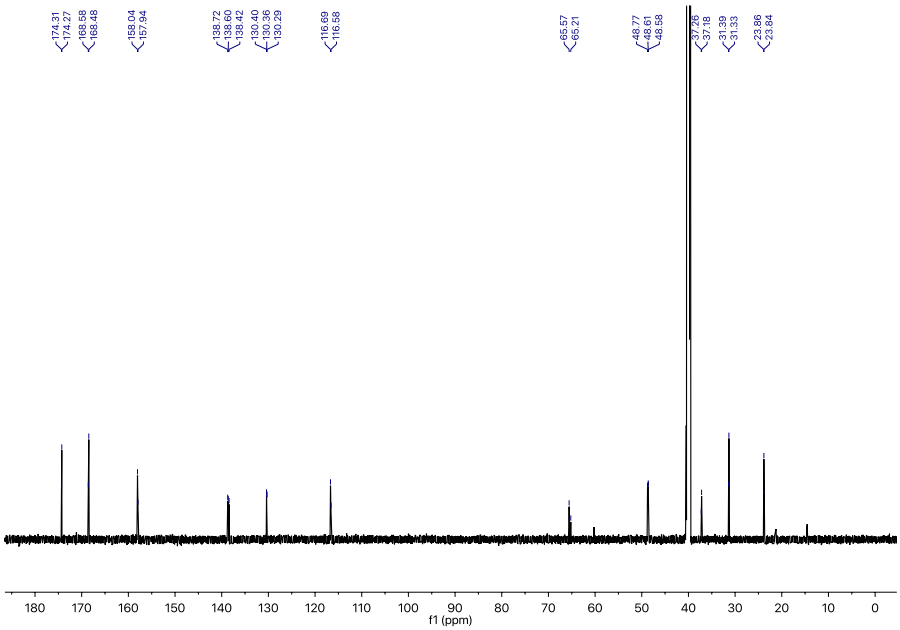

Figure S6. ^{13}C NMR spectrum (213 MHz, 298 K) of 2 mM $\mathbf{2}_{anti}$ in $(CD_3)_2SO$.

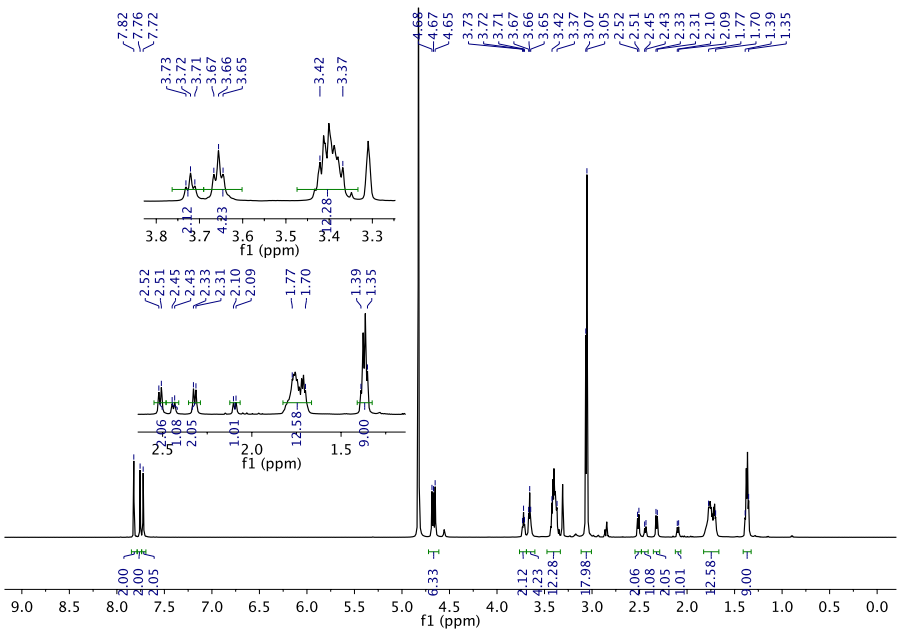

Figure S7. ^{1}H NMR spectrum (600 MHz, 298 K) of 2 mM $\mathbf{3}_{anti}$ in CD_3OD.

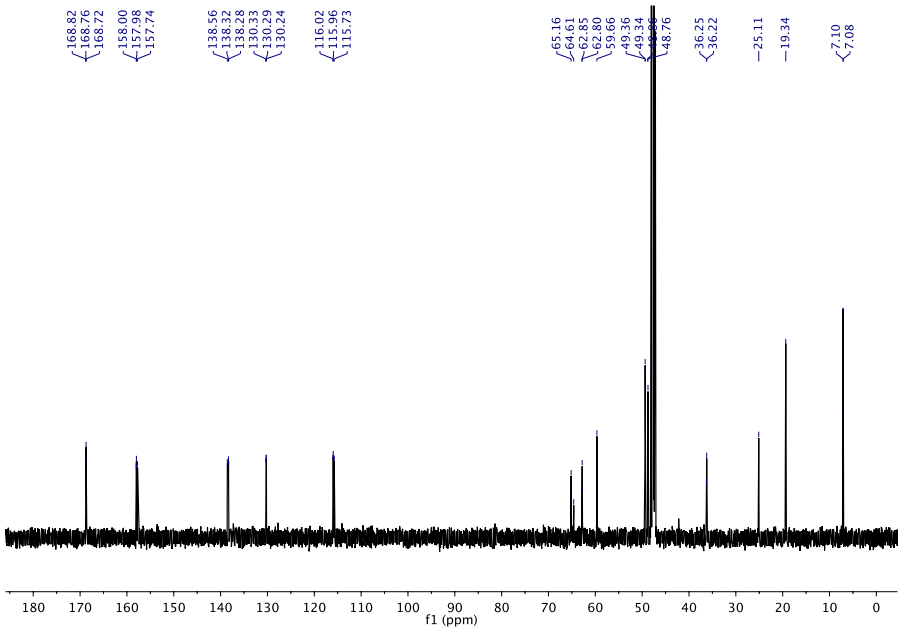

Figure S8. ^{13}C NMR spectrum (150 MHz, 298 K) of 2 mM $\mathbf{3}_{anti}$ in CD_3OD.

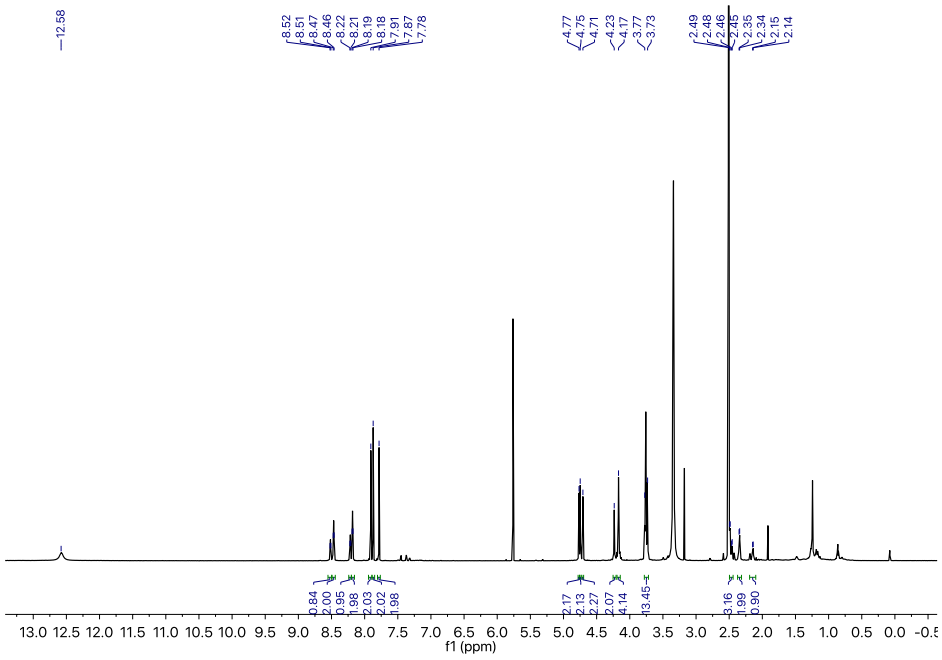

Figure S9. ^{1}H NMR spectrum (850 MHz, 298 K) of **8**$_{anti}$ in $(CD_3)_2SO$.

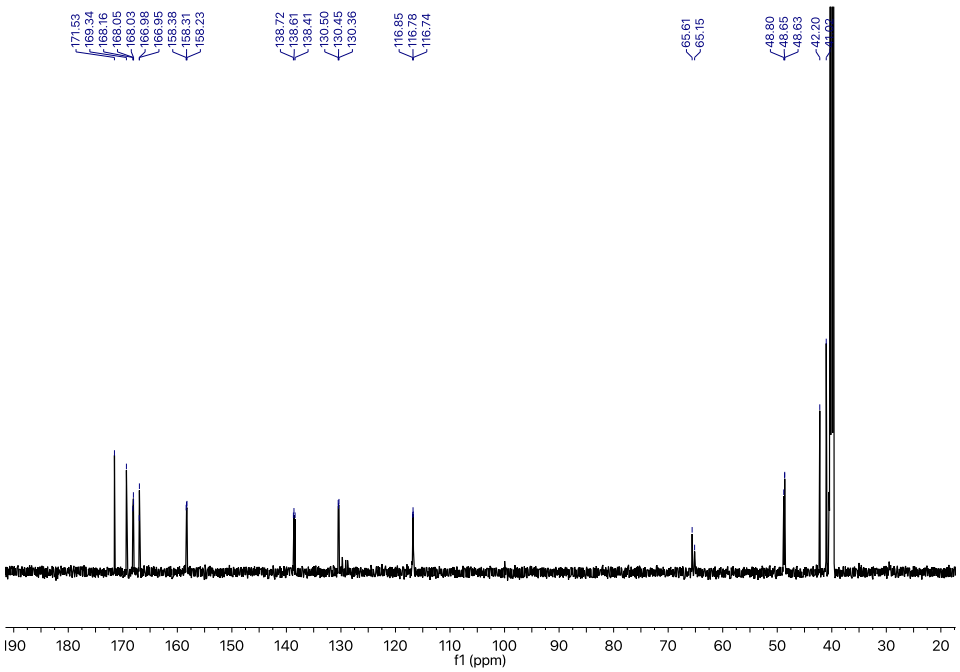

Figure S10. ^{13}C NMR spectrum (175 MHz, 298 K) of **8**$_{anti}$ in $(CD_3)_2SO$.

^{1}H NMR Spectroscopic and ESI-MS Experiments

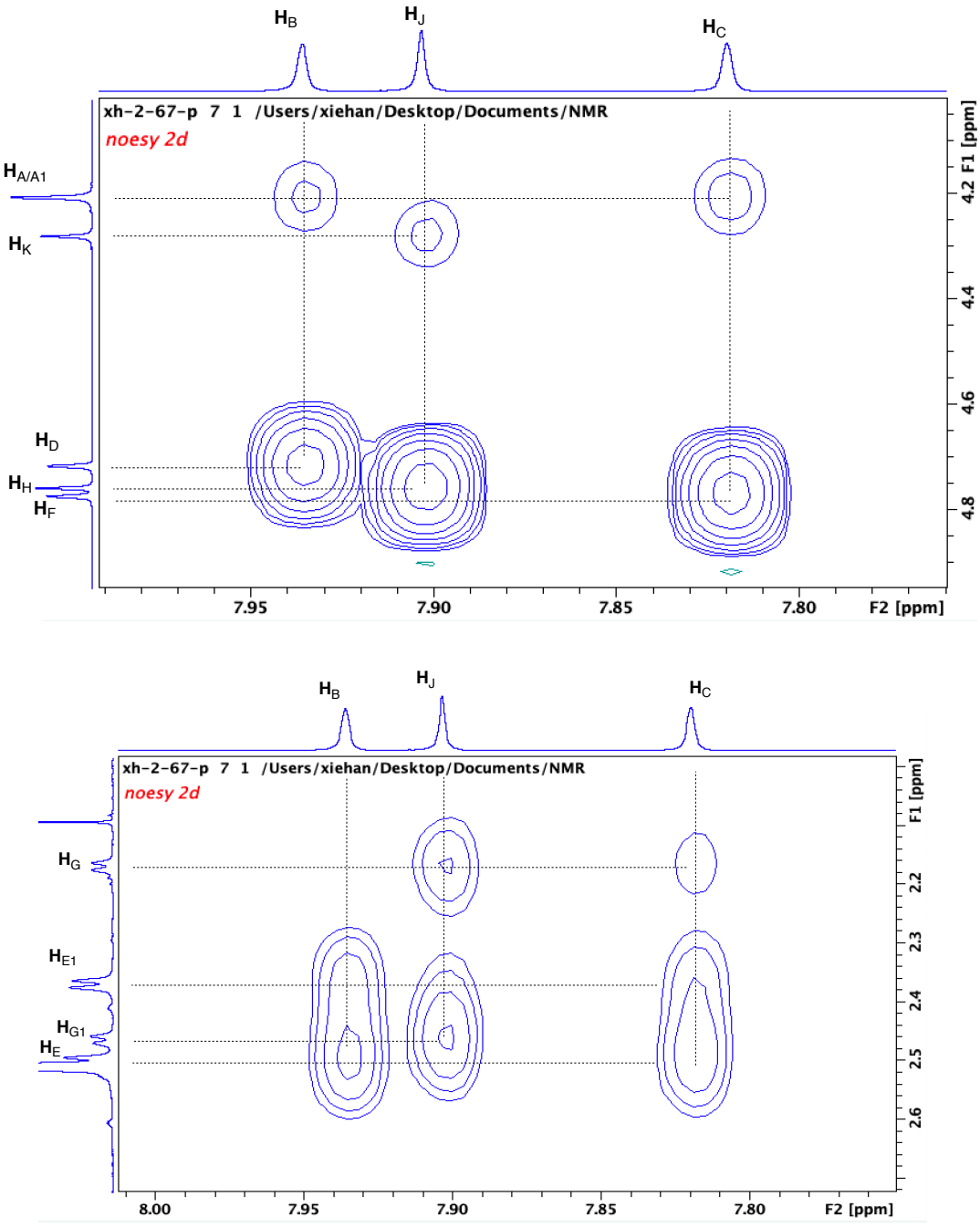

Figure S11. Two regions of 2D NOESY NMR spectrum (600 MHz, 298 K) of 5.0 mM solution of $\mathbf{1}_{anti}$ in $(CD_3)_2SO$ showing important cross-correlations. We used the integration ratio of $\mathbf{H}_{A/A1}$ and $\mathbf{H}_K$ resonances to distinguish these protons and then as a starting point to assign other nuclei.

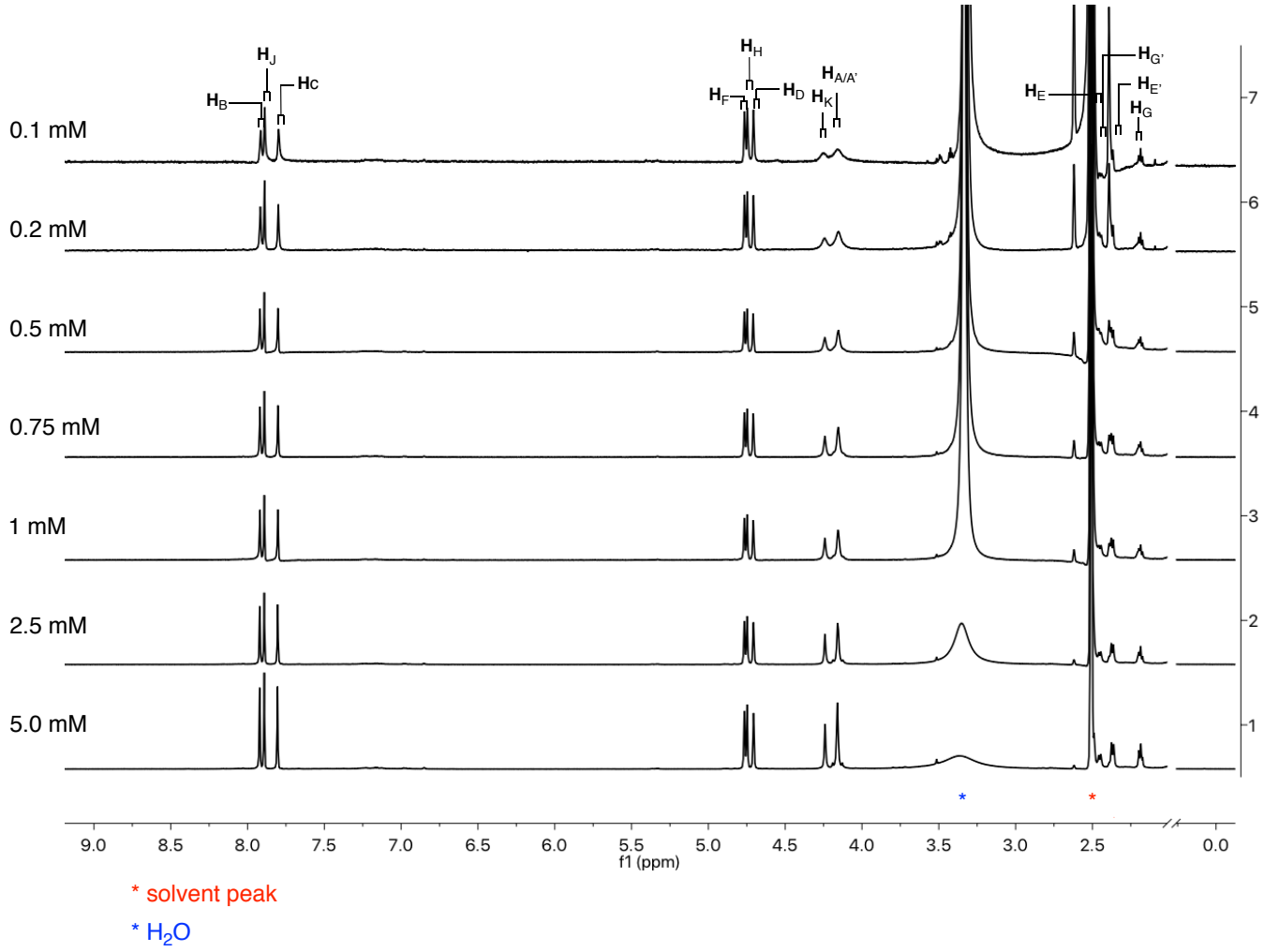

Figure S12. ^{1}H NMR spectra (600 MHz, 298 K) of 5.0 mM **1**$_{anti}$ in $(CD_3)_2SO$ (bottom) and its more diluted solutions (concentrations are shown on the left).

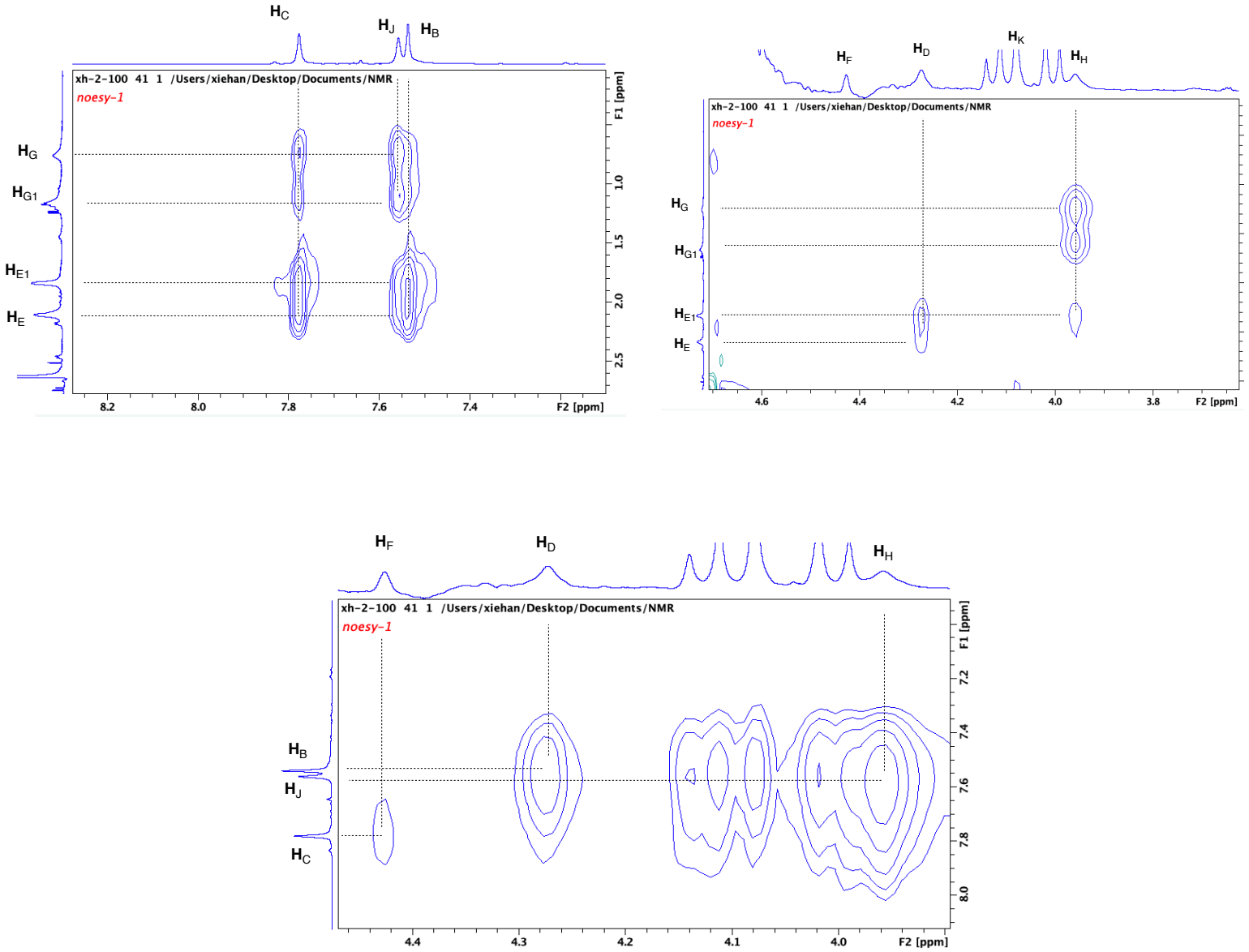

Figure S13. Selected regions of 2D NOESY NMR spectrum (600 MHz, 298 K) of 5.0 mM solution (H_2O: D_2O = 9:1, 0.1 M phosphate salts and 0.1 M NaCl) of $[\mathbf{1}_{anti}]^{3-}$ at pH = 7.2. We used the integration ratio of $\mathbf{H}_{E/E1}$ and $\mathbf{H}_{G/G1}$ resonances to distinguish them and then assign the remaining nuclei.

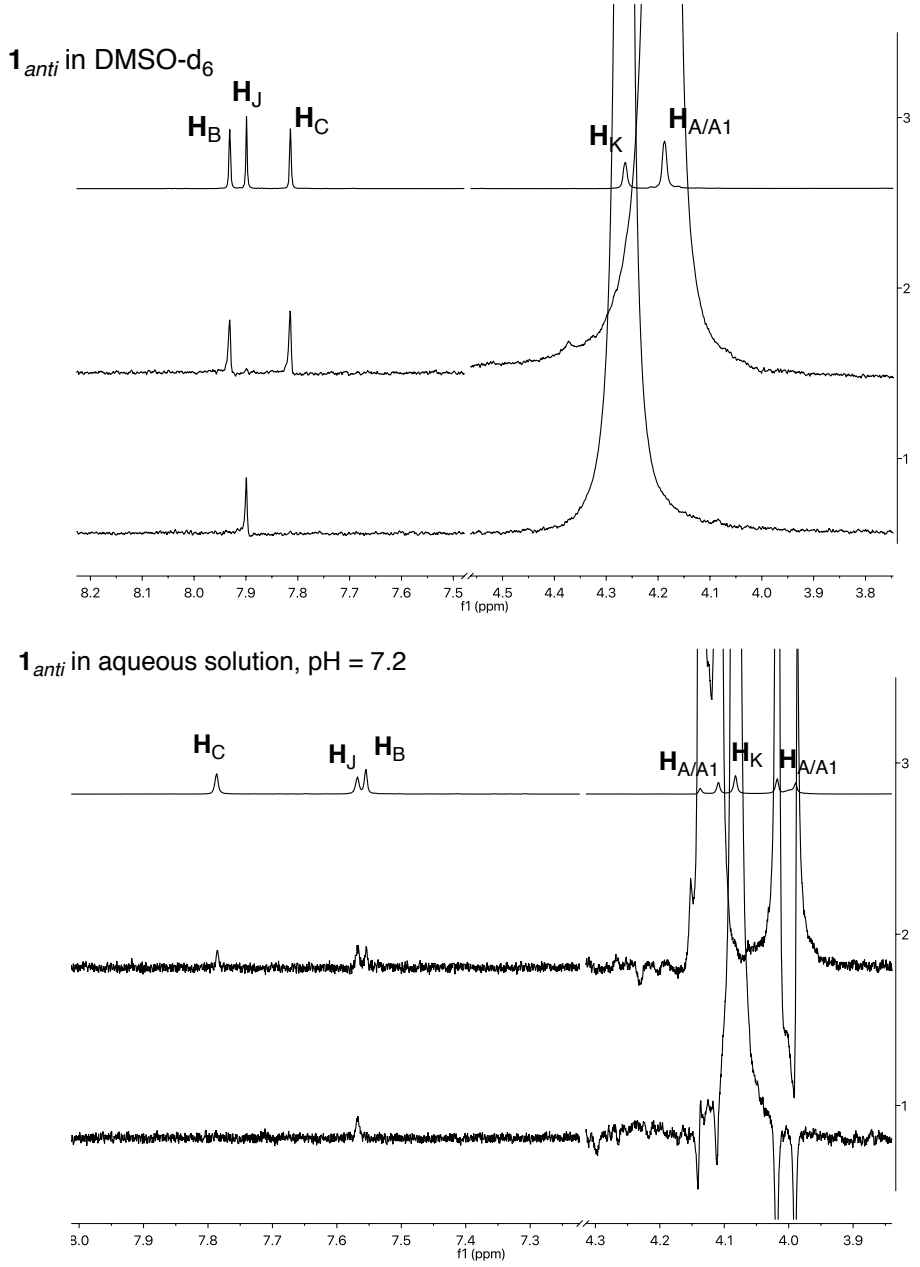

Figure S14. 1D NOE spectra (600 MHz, 298 K) of 5.0 mM solution of $\mathbf{1}_{anti}$ in DMSO-d_6 (top) and $[\mathbf{1}_{anti}]_2^{3-}$ in water (H_2O: D_2O = 9:1, 0.1 M phosphate salts and 0.1 M NaCl, bottom) obtained after the selective irradiation of $\mathbf{H}_{A/A1}$ (middle spectrum in each set) and $\mathbf{H}_K$ (bottom spectrum in each set) resonances.

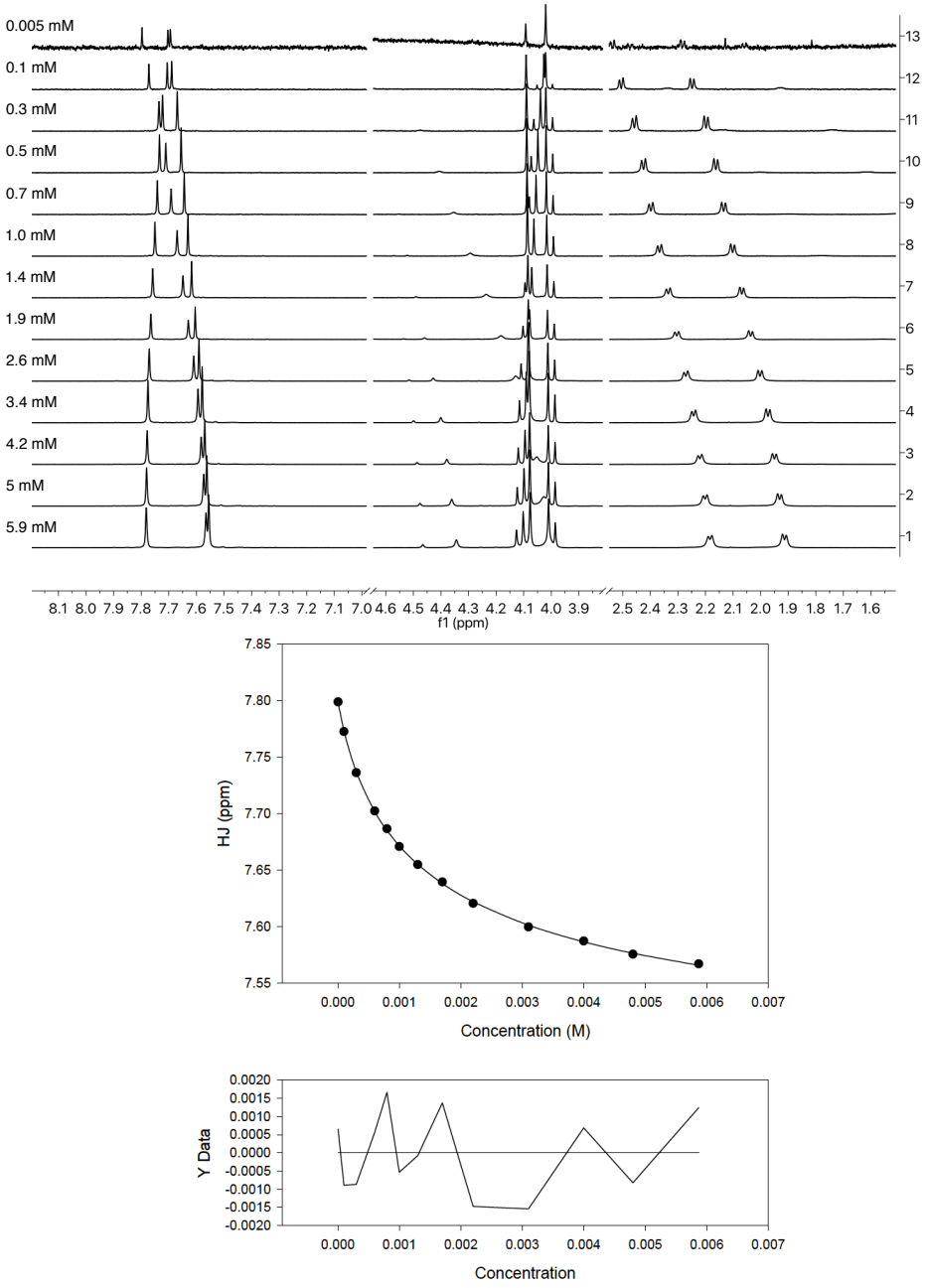

Figure S15. (Top) ^{1}H NMR spectra (600 MHz, 298 K) of $[\mathbf{1}_{anti}]^{3-}$ at different concentrations (shown on the left) in 0.1 M phosphate buffer at pH = 7.2. (Bottom) Nonlinear least-square analysis of ^{1}H NMR binding data corresponding to the formation of homodimer $[\mathbf{1}_{anti}]_2^{6-}$. Using the change in chemical shift of $\mathbf{H}_J$ as a function of the overall concentration of $[\mathbf{1}_{anti}]^{3-}$ we obtained stability constant K_a = 410 ± 10 M^{-1} (SigmaPlot) as arithmetic mean of two separate measurements with the standard deviation as error. A random distribution of residuals is shown at the bottom.

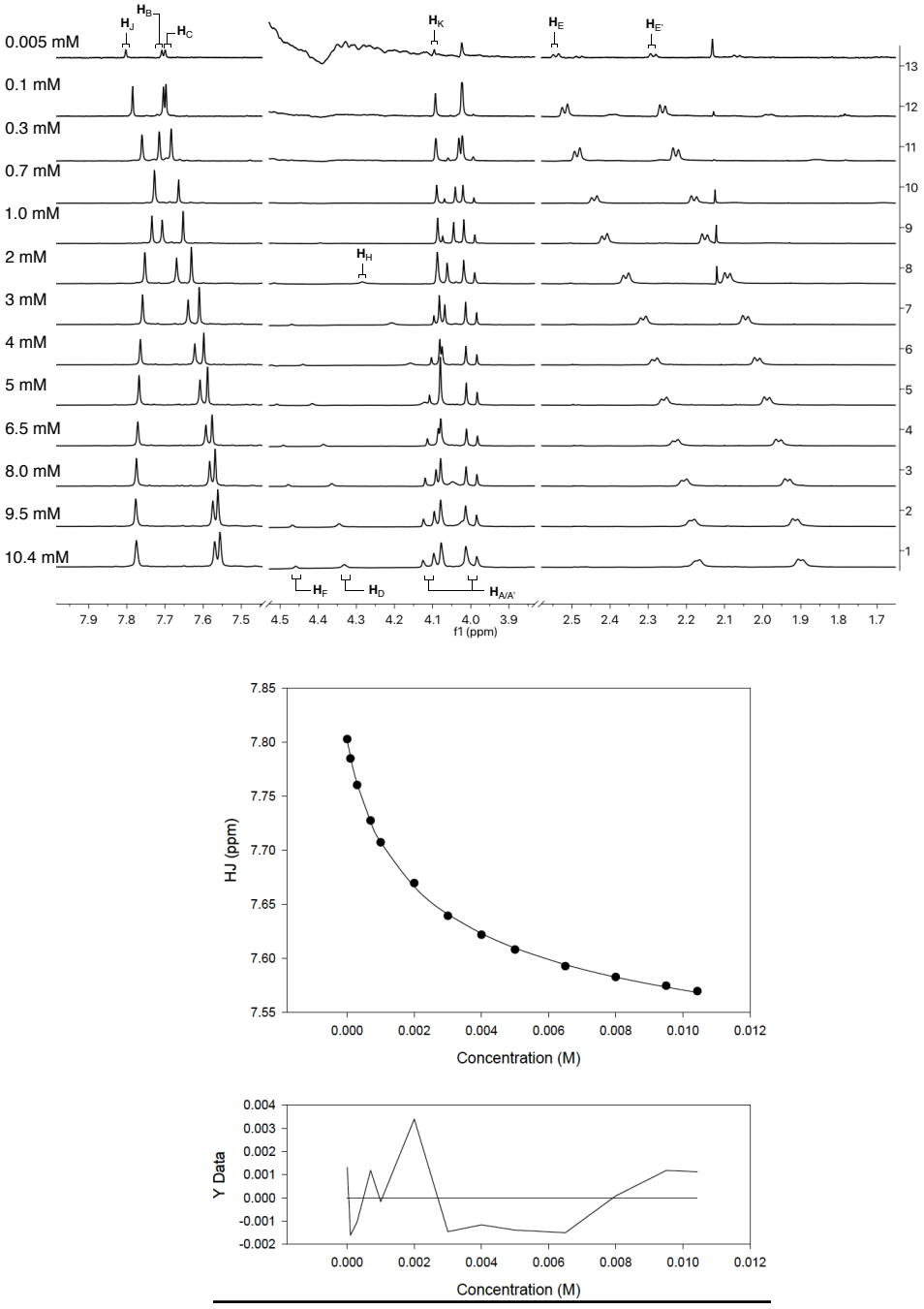

Figure S16. (Top) ^{1}H NMR spectra (600 MHz, 298 K) of $[\mathbf{1}_{anti}]^{3-}$ at different concentrations (shown on the left) in 25 mM phosphate buffer at pH = 7.2. (Bottom). Nonlinear least-square analysis of ^{1}H NMR binding data corresponding to the formation of homodimer $[\mathbf{1}_{anti}]_2^{6-}$. Using the change in chemical shift of $\mathbf{H}_J$ as a function of the overall concentration (one shown in Figure 4B, and another one here) of $[\mathbf{1}_{anti}]^{3-}$ we obtained stability constant $K_a = 152 \pm 60$ M^{-1} (SigmaPlot) as an arithmetic mean of three separate measurements with the standard deviation as error. A random distribution of residuals is shown at the bottom.

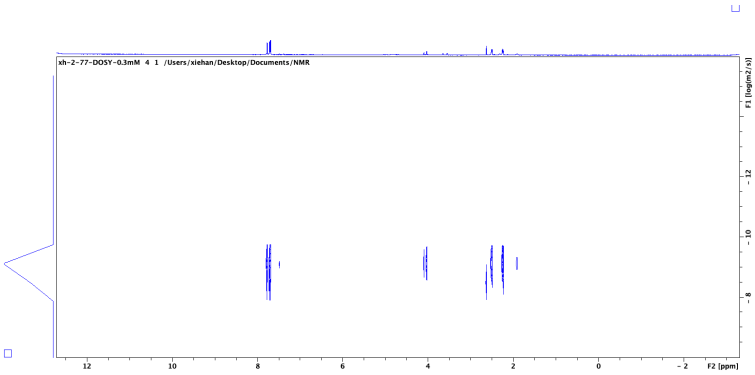
xh-2-77-DOSY-0.3mM 4 1 /Users/xiehan/Desktop/Documents/NMR
F1 [log(m2/s)]
F2 [ppm]

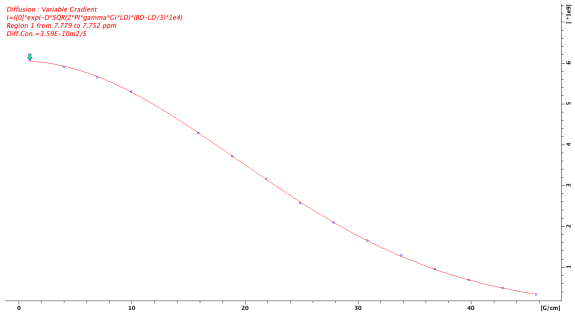
Diffusion : Variable Gradient
I=I[0]*exp(-D*SQR(2*PI*gamma*Gi*LD)*(BD-LD/3)*1e4)
Region 1 from 7.779 to 7.752 ppm
Diff.Con.=3.19E-10m2/S
[G/cm]

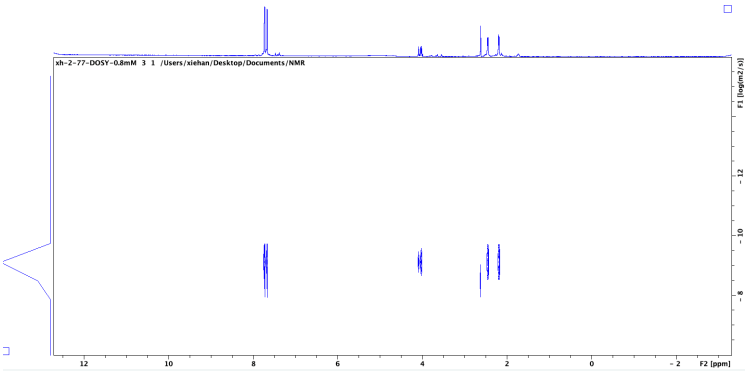
xh-2-77-DOSY-0.8mM 3 1 /Users/xiehan/Desktop/Documents/NMR
F1 [log(m2/s)]
F2 [ppm]

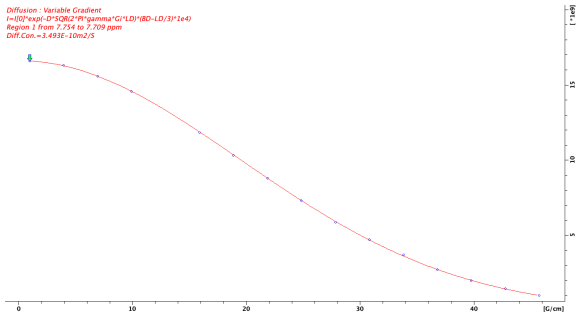
Diffusion : Variable Gradient
I=I[0]*exp(-D*SQR(2*PI*gamma*Gi*LD)*(BD-LD/3)*1e4)
Region 1 from 7.754 to 7.709 ppm
Diff.Con.=3.493E-10m2/S
[G/cm]

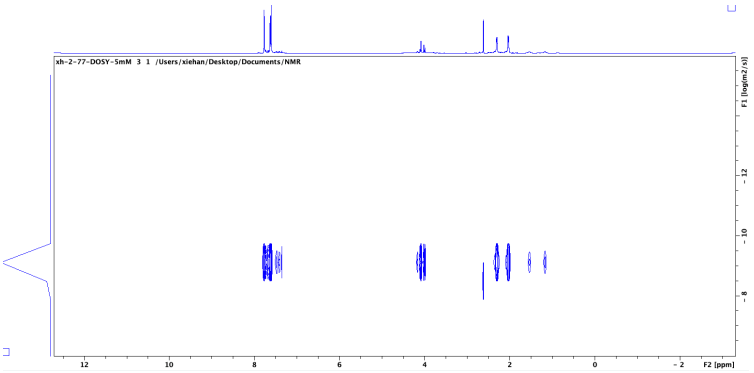
xh-2-77-DOSY-5mM 3 1 /Users/xiehan/Desktop/Documents/NMR
F1 [log(m2/s)]
F2 [ppm]

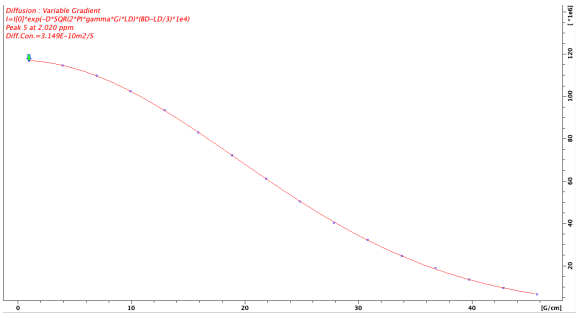
Diffusion : Variable Gradient
I=I[0]*exp(-D*SQR(2*PI*gamma*Gi*LD)*(BD-LD/3)*1e4)
Peak 5 at 2.020 ppm
Diff.Con.=3.149E-10m2/S
[G/cm]

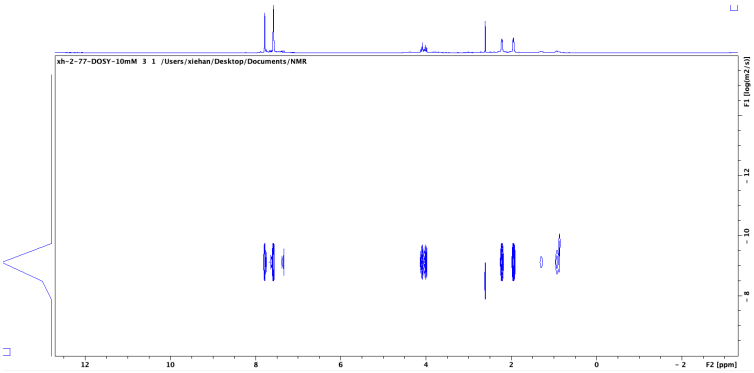
xh-2-77-DOSY-10mM 3 1 /Users/xiehan/Desktop/Documents/NMR
F1 [log(m2/s)]
F2 [ppm]

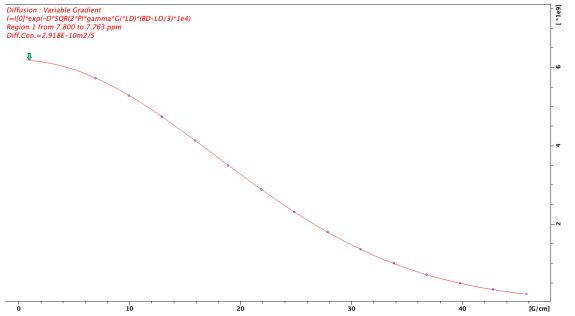
Diffusion : Variable Gradient
I=I[0]*exp(-D*SQR(2*PI*gamma*Gi*LD)*(BD-LD/3)*1e4)
Region 1 from 7.800 to 7.763 ppm
Diff.Con.=2.918E-10m2/S
[G/cm]

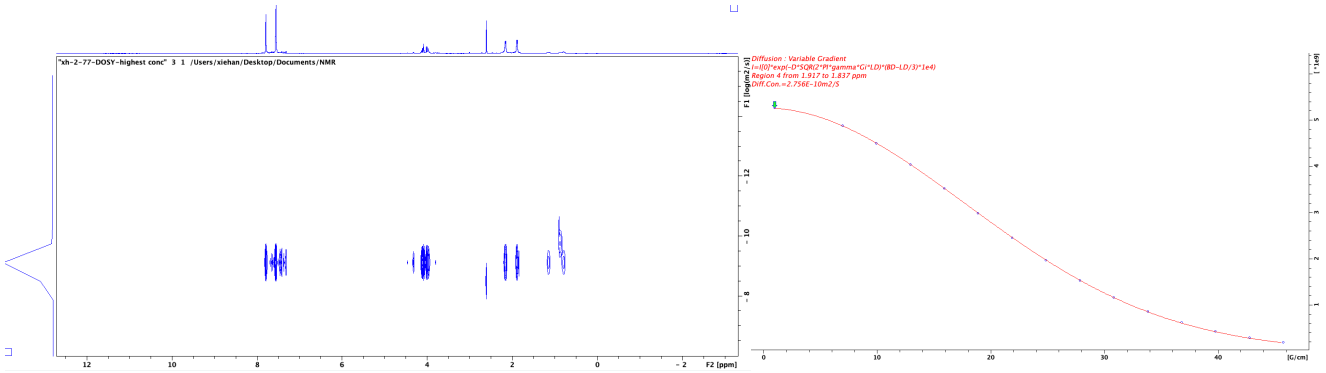

Figure S17. (Left) DOSY NMR spectra (600 MHz, 298 K) of $[\mathbf{1}_{anti}]^{3-}$ in 25 mM phosphate buffer (H_2O: D_2O = 9:1) at pH = 7.2. (Right) The change in intensity of resonance corresponding to $\mathbf{H}_J$ proton as a function of the field gradient g (G/cm) was obtained using the pulse field gradient stimulated echo sequence with bipolar gradient pulse pair, 1 spoil gradient, 3-9-19 WATERGATE solvent suppression (stebpgp1s19) pulse sequence and the data was fit to the Stejskal-Tanner equation to give the value of diffusion coefficient D_{app} (m^2/s); The hydrodynamic radii was computed using the Stokes-Einstein equation whereby the viscosity of 25 mM phosphate buffer at pH = 7.2 ± 0.1 is assumed to be similar to that of H_2O:D_2O = 9:1 (η = 0.91 mPa s at 298.1). From top to bottom, the overall concentration of $[\mathbf{1}_{anti}]^{3-}$ and D_{app} are as follows: (A) 0.3 mM, $D_{app} = 3.59\times10^{-10}$ m^2s^{-1} (B) 0.8 mM, $D_{app} = 3.49\times10^{-10}$ m^2s^{-1} (C) 5.0 mM, $D_{app} = 3.15\times10^{-10}$ m^2s^{-1} (D) 10.0 mM, $D_{app} = 2.92\times10^{-10}$ m^2s^{-1} (E) 15.7 mM, $D_{app} = 2.76\times10^{-10}$ m^2s^{-1}.

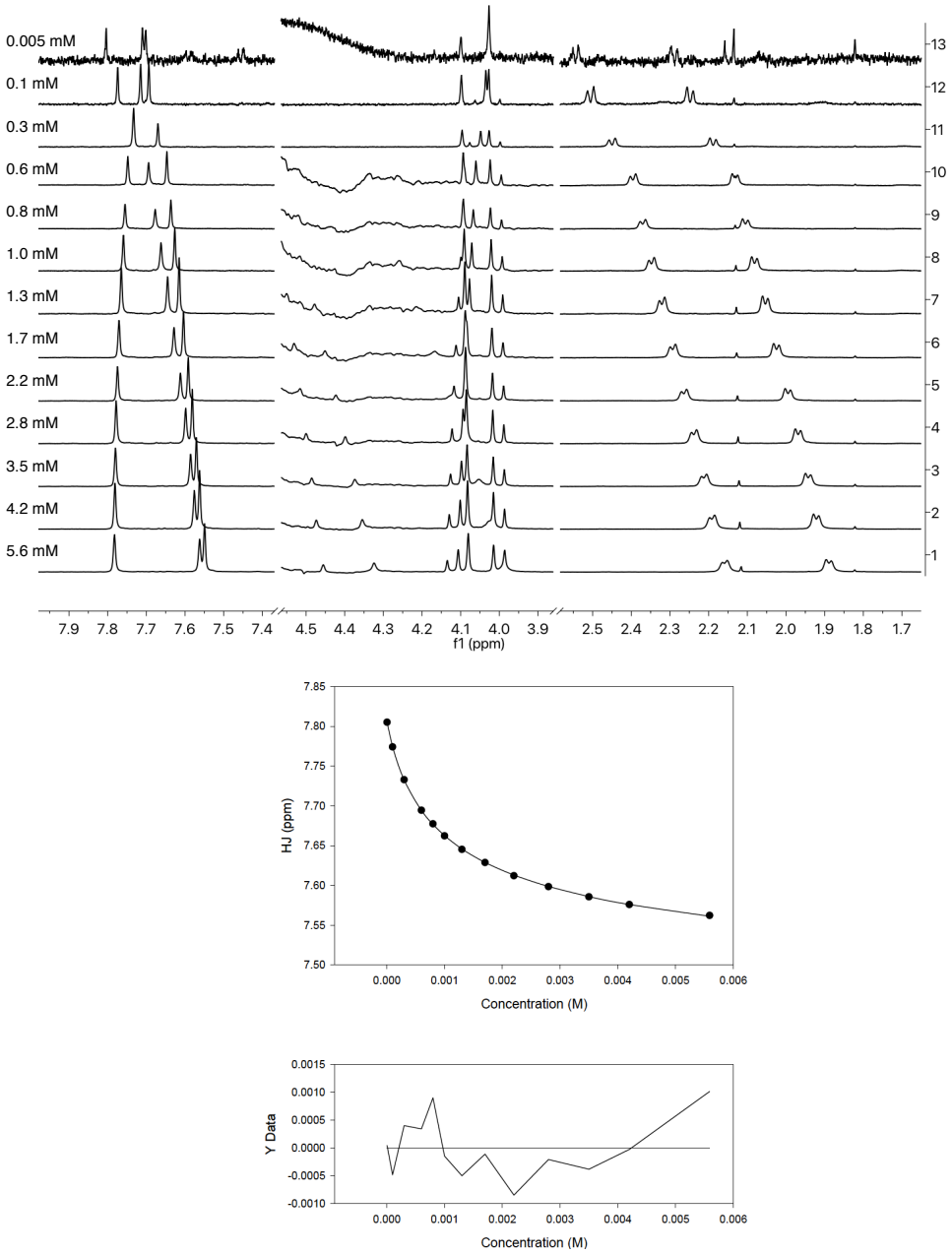

Figure S18. (Top) ^{1}H NMR spectra (600 MHz, 298 K) of $[\mathbf{1}_{anti}]^{3-}$ at different concentrations (shown on the left) in 0.1 M phosphate buffer containing 0.1 M NaCl at pH = 7.2. (Bottom). Nonlinear least-square analysis of ^{1}H NMR binding data corresponding to the formation of homodimer $[\mathbf{1}_{anti}]_2^{6-}$. Using the change in chemical shift of $\mathbf{H}_J$ as a function of the overall concentration of $[\mathbf{1}_{anti}]^{3-}$ we obtained stability constant K_a = 570 ± 62 M^{-1} (SigmaPlot) as an arithmetic mean of two separate measurements with the standard deviation as error. A random distribution of residuals is shown at the bottom.

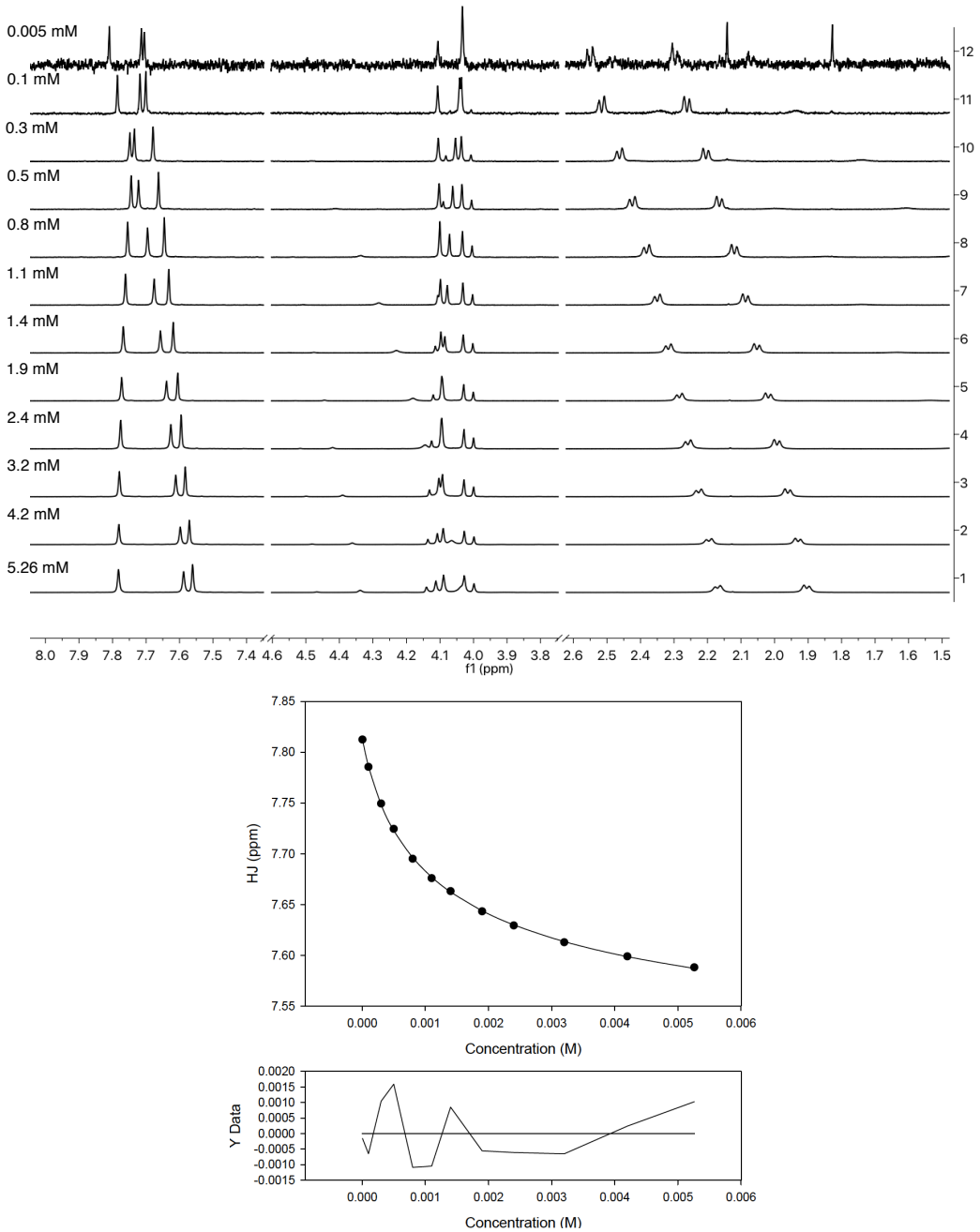

Figure S19. (Top) ^{1}H NMR spectra (600 MHz, 298 K) of $[\mathbf{1}_{anti}]^{3-}$ at different concentrations (shown on the left) in 0.1 M phosphate buffer containing 0.1 M $NaClO_4$ at pH = 7.2. (Bottom). Nonlinear least-square analysis of ^{1}H NMR binding data corresponding to the formation of homodimer $[\mathbf{1}_{anti}]_2^{6-}$. Using the change in chemical shift of $\mathbf{H}_J$ as a function of the overall concentration of $[\mathbf{1}_{anti}]^{3-}$ we obtained stability constant K_a = 458 ± 11 M^{-1} (SigmaPlot) as an arithmetic mean of two separate measurements with the standard deviation as error. A random distribution of residuals is shown at the bottom.

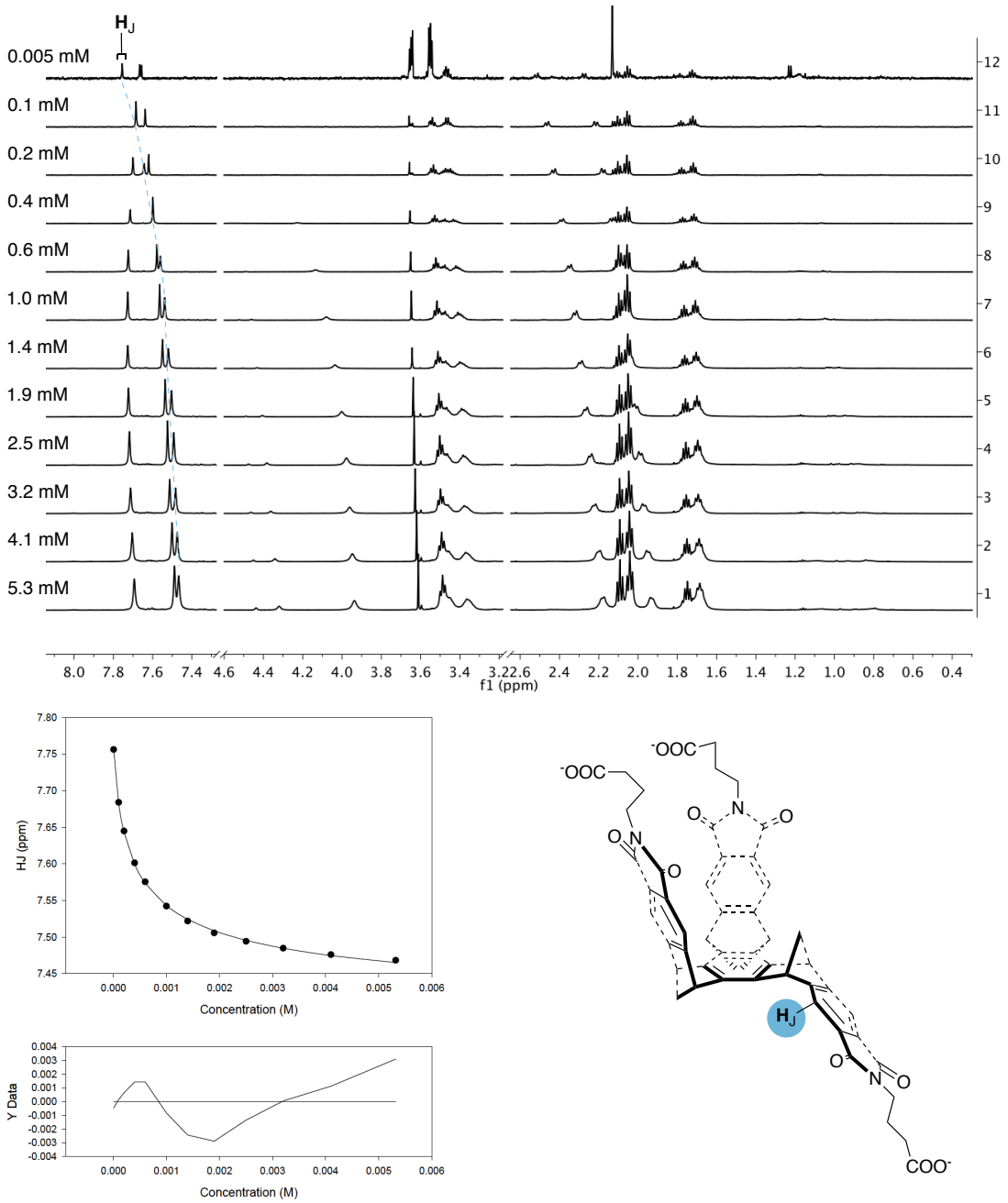

Figure S20. (Top) ^{1}H NMR spectra (600 MHz, 298 K) of $[\mathbf{2}_{anti}]^{3-}$ at different concentrations (shown on the left) in 25 mM phosphate buffer at pH = 7.2. (Bottom). Nonlinear least-square analysis of ^{1}H NMR binding data corresponding to the formation of homodimer $[\mathbf{2}_{anti}]_2^{6-}$. Using the change in chemical shift of $\mathbf{H}_J$ as a function of the overall concentration of $[\mathbf{2}_{anti}]^{3-}$ we obtained stability constant $K_a = 1704 \pm 42$ M^{-1} (SigmaPlot) as an arithmetic mean of two separate measurements with the standard deviation as error. A distribution of residuals is shown at the bottom.

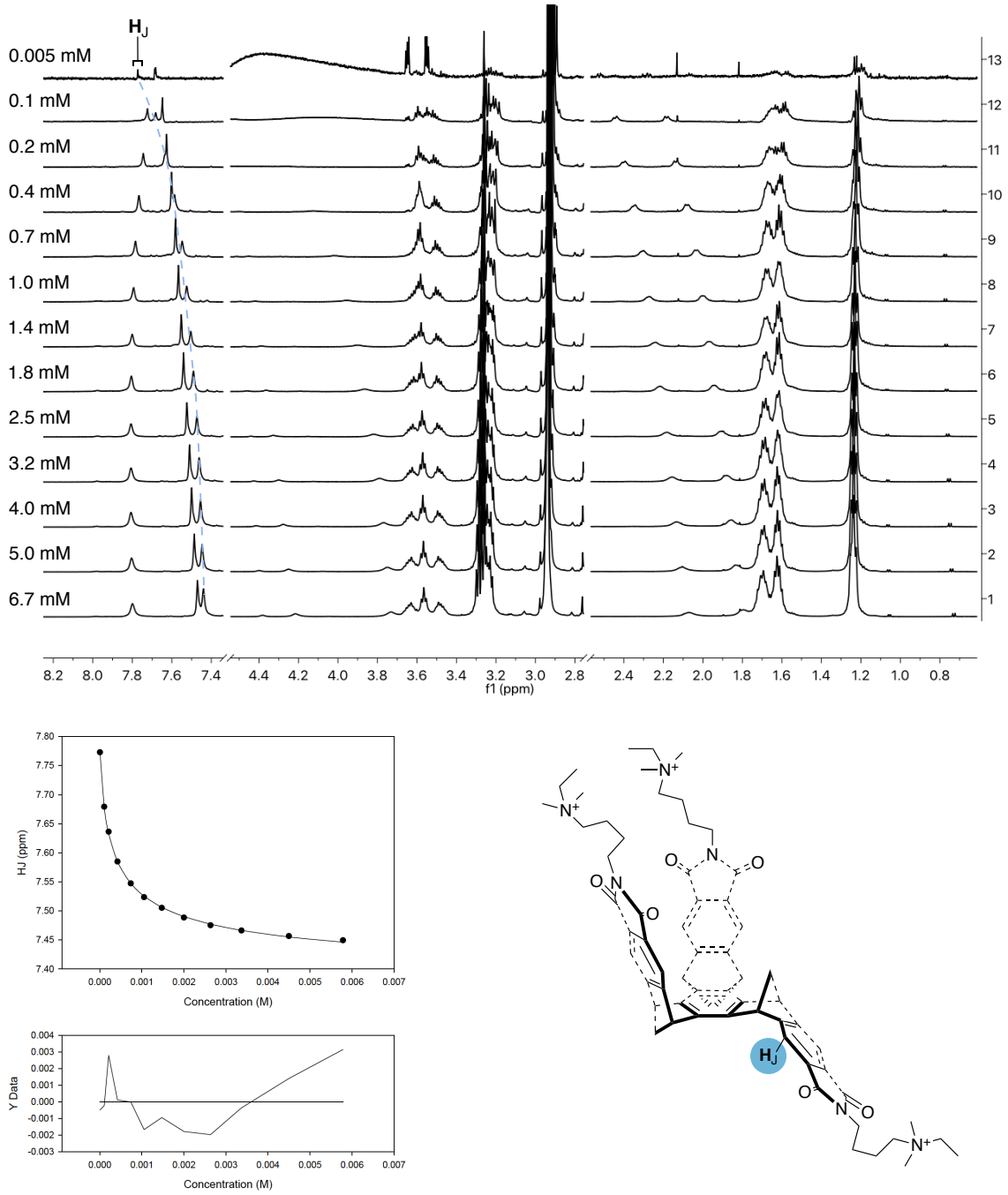

Figure S21. (Top) ^{1}H NMR spectra (600 MHz, 298 K) of $[\mathbf{3}_{anti}]^{3+}$ at different concentrations (shown on the left) in 25 mM phosphate buffer at pH = 7.2. (Bottom). Nonlinear least-square analysis of ^{1}H NMR binding data corresponding to the formation of homodimer $[\mathbf{3}_{anti}]_2^{6+}$. Using the change in chemical shift of $\mathbf{H}_J$ as a function of the overall concentration of $[\mathbf{3}_{anti}]^{3+}$ we obtained stability constant $K_a = 1704 \pm 42$ M^{-1} (SigmaPlot) as an arithmetic mean of two separate measurements with the standard deviation as error. A distribution of residuals is shown at the bottom.

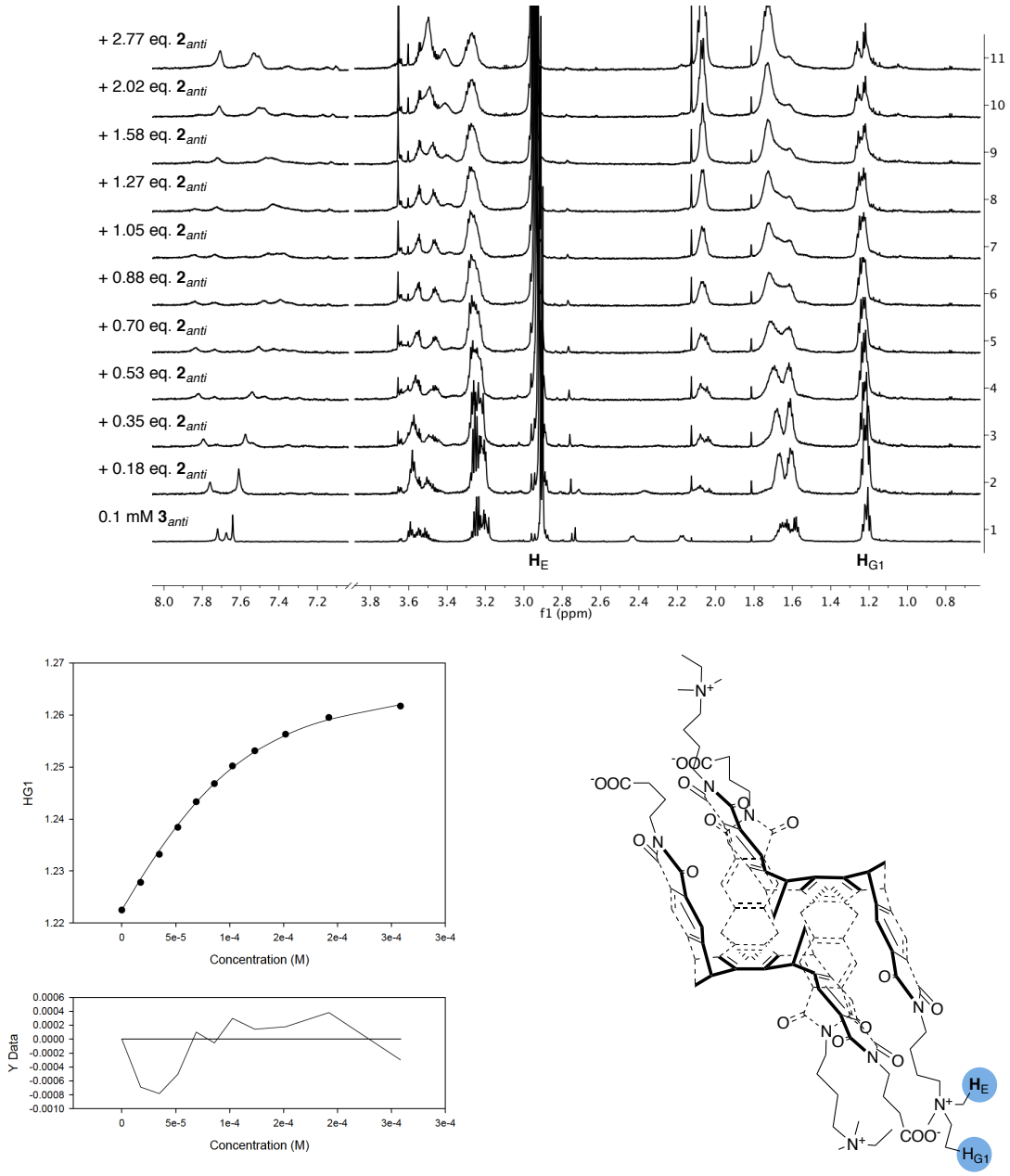

Figure S22. (Top) ^{1}H NMR spectra (600 MHz, 298 K) of 0.1 mM of $[\mathbf{3}_{anti}]^{3+}$ in 25 mM phosphate buffer at pH = 7.2, obtained upon an incremental addition of 4.0 mM solution of $[\mathbf{2}_{anti}]^{3-}$ (Bottom). Nonlinear least-square analysis of ^{1}H NMR binding data corresponding to the formation of $[\mathbf{2}_{anti}\subset\mathbf{3}_{anti}]$ (1:1) complex. Using the change in chemical shift of $\mathbf{H}_{G1}$ as a function of the overall concentration of $[\mathbf{2}_{anti}]^{3-}$ we obtained stability constant $K_a = 3.3 \pm 0.2 \cdot 10^4\ M^{-1}$ (SigmaPlot) as an arithmetic mean of two separate measurements with the standard deviation as error; note that homodimerization of $[\mathbf{3}_{anti}]^{3+}$ (in addition to $[\mathbf{2}_{anti}]^{3-}$) was negligible under the experimental conditions, and therefore not included in the theoretical model. A distribution of residuals is shown at the bottom.

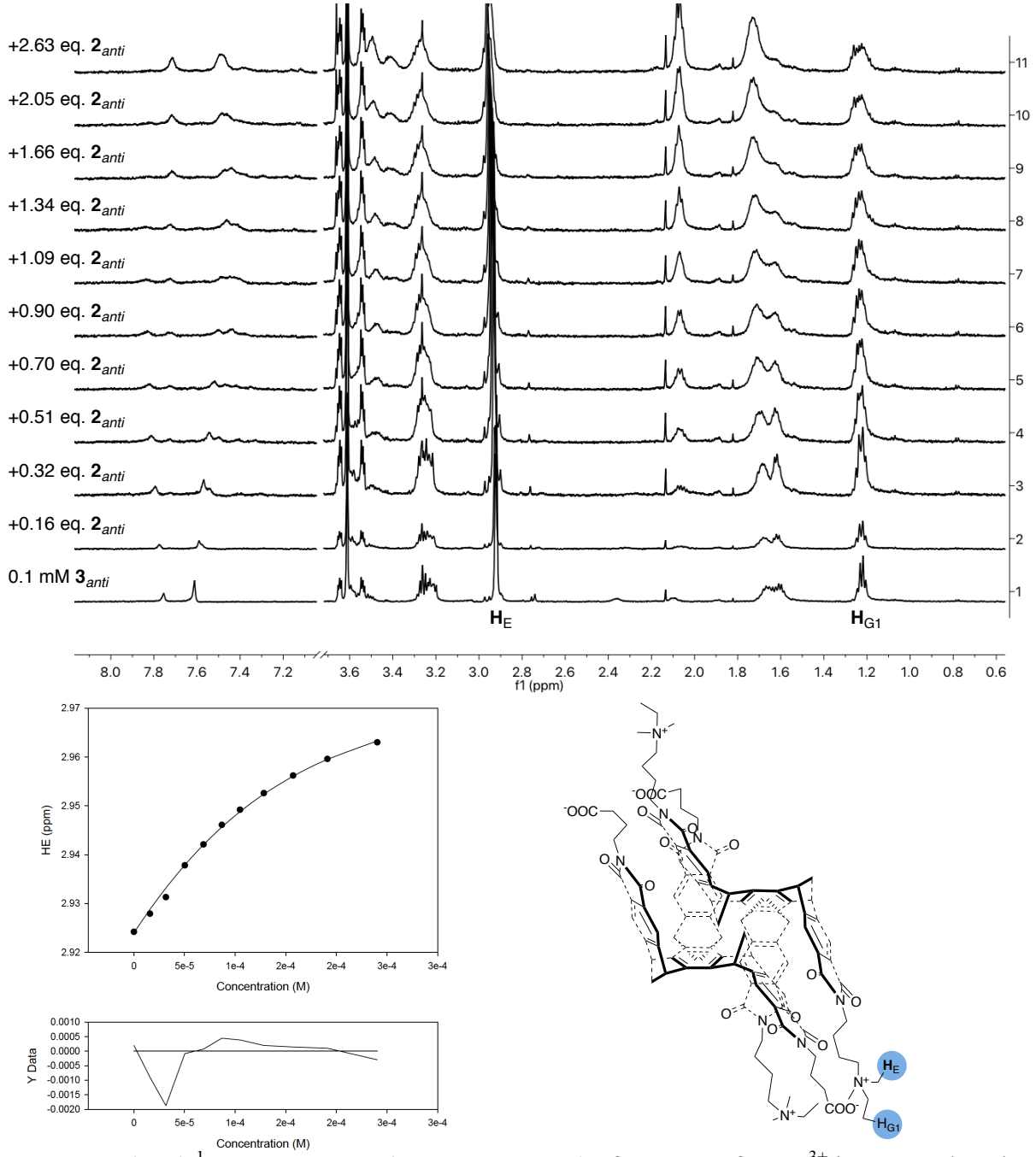

Figure S23. (Top) ^{1}H NMR spectra (600 MHz, 298 K) of 0.1 mM of $[\mathbf{3}_{anti}]^{3+}$ in 0.1 M phosphate buffer with 0.1 M NaCl at pH = 7.2, obtained upon an incremental addition of 4.0 mM solution of $[\mathbf{2}_{anti}]^{3-}$ (Bottom). Nonlinear least-square analysis of ^{1}H NMR binding data corresponding to the formation of $[\mathbf{2}_{anti}\subset\mathbf{3}_{anti}]$ (1:1) complex. Using the change in chemical shift of $\mathbf{H}_{E}$ as a function of the overall concentration of $[\mathbf{2}_{anti}]^{3-}$ we obtained stability constant $K_a = 1.3 \pm 0.2 \cdot 10^4$ M^{-1} (SigmaPlot) as an arithmetic mean of two separate measurements with the standard deviation as error; note that homodimerization of $[\mathbf{3}_{anti}]^{3+}$ (in addition to $[\mathbf{2}_{anti}]^{3-}$) was negligible under the experimental conditions, and therefore not included in the theoretical model. A distribution of residuals is shown at the bottom.

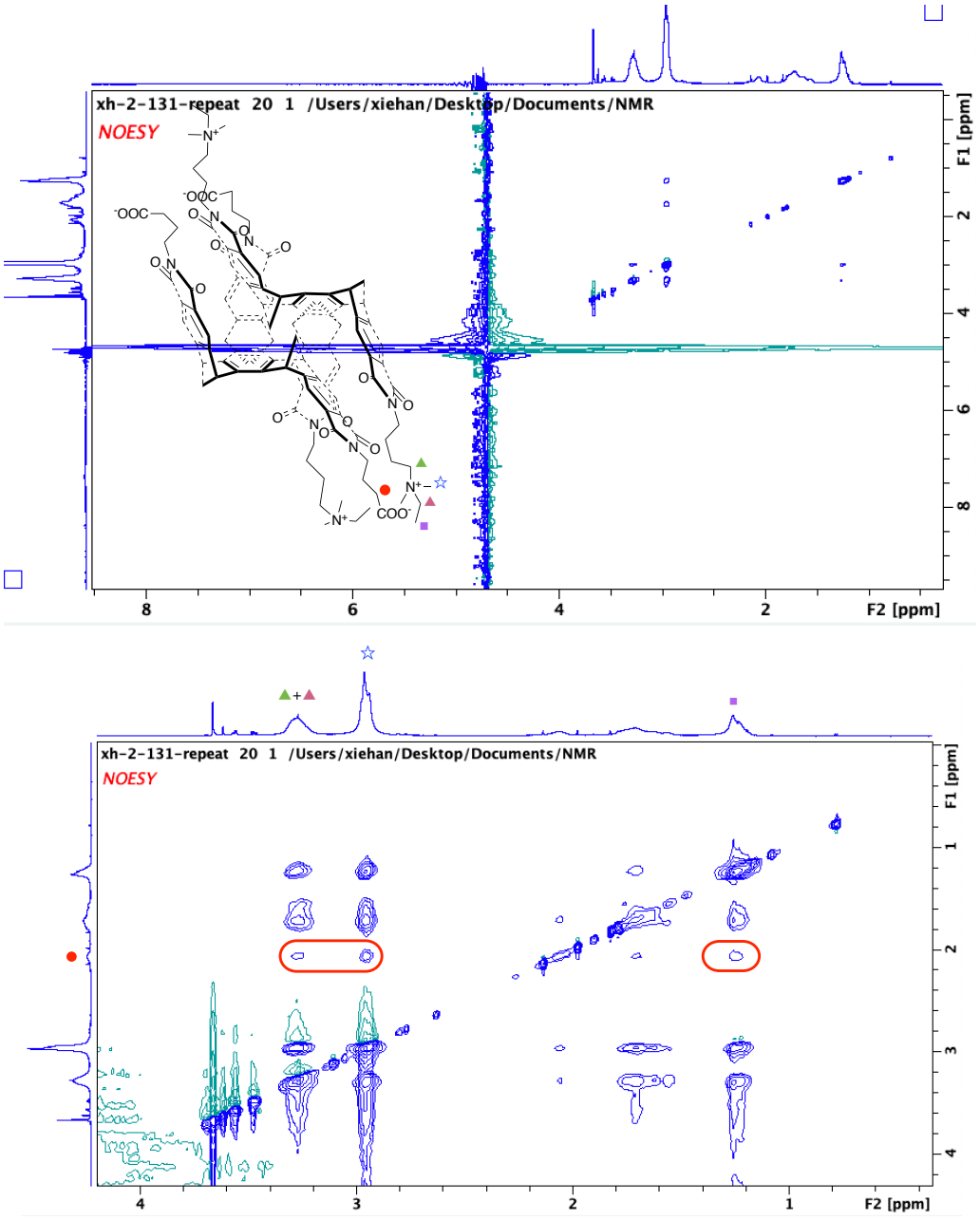

Figure S24. Two views of 2D NOESY NMR spectrum (600 MHz, 298 K) of 1.0 mM heterodimer [$\mathbf{2}_{anti}\subset\mathbf{3}_{anti}$] ($H_2O$: D_2O = 9:1) in 25 mM phosphate buffer at pH = 7.2. Intermolecular cross-correlations suggesting the proposed geometry of [$\mathbf{2}_{anti}\subset\mathbf{3}_{anti}$] complex are depicted with colored symbols (triangles, circle, star and square).

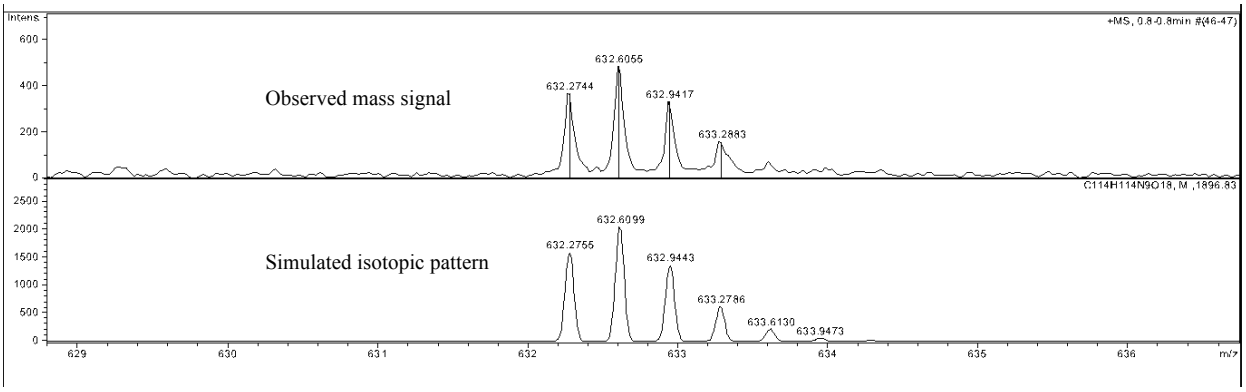

Figure S25. Segments of experimental (top) and simulated (bottom) high-resolution ESI-Mass spectra of [$\mathbf{2}_{anti}\subset\mathbf{3}_{anti}$], suggesting the formation of [$\mathbf{2}_{anti}\subset\mathbf{3}_{anti}-3\mathrm{Br}]^{3+}$ cation with *m*/*z* calcd for $C_{114}H_{114}N_9O_{18}^{3+}$ 632.2755 (bottom) and found 632.2744 (top).

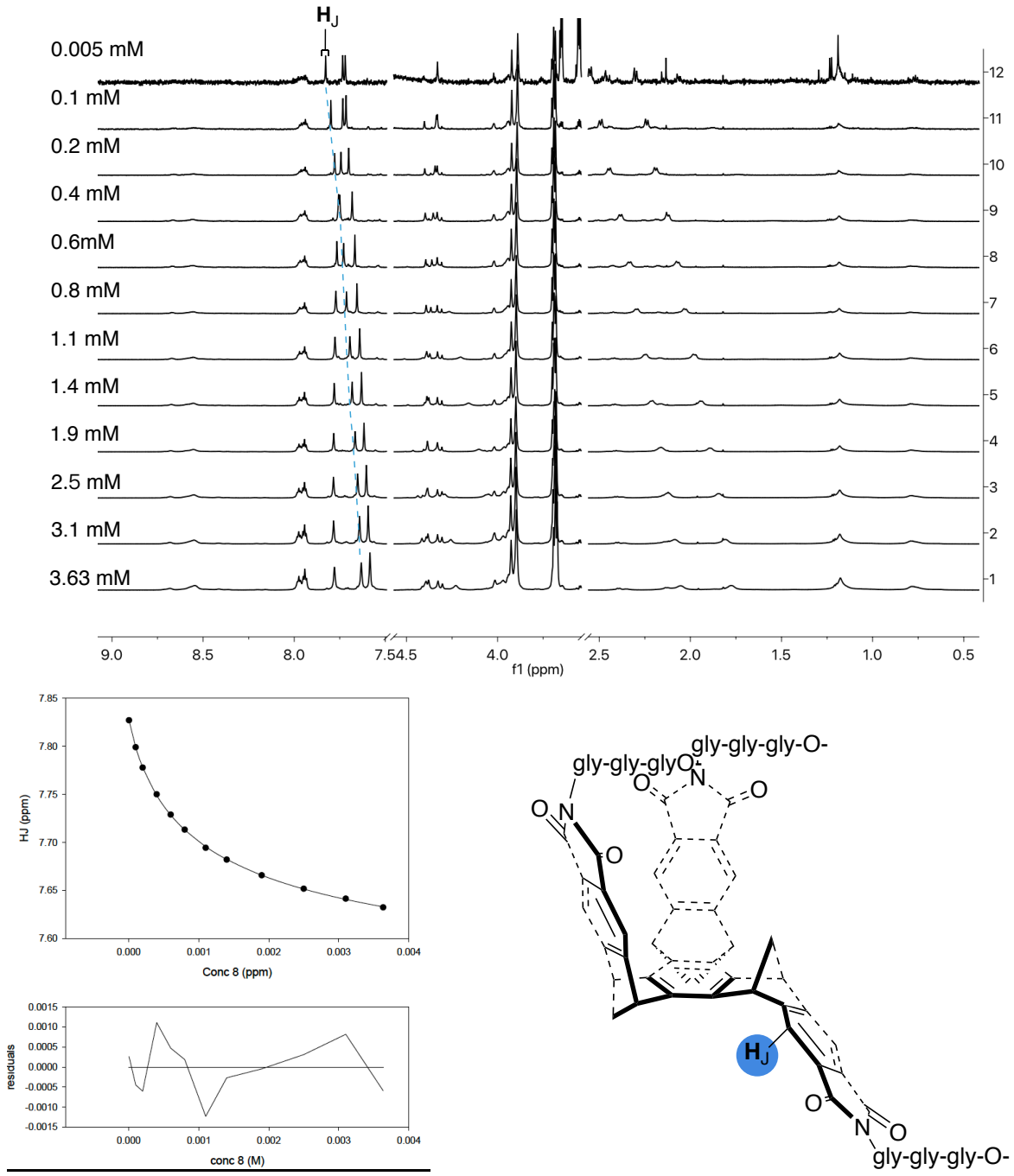

Figure S26. (Top) ^{1}H NMR spectra (600 MHz, 298 K) of $[\mathbf{8}_{anti}]^{3-}$ at different concentrations (shown on the left) in 25 mM phosphate buffer at pH = 7.2. (Bottom). Nonlinear least-square analysis of ^{1}H NMR binding data corresponding to the formation of homodimer $[\mathbf{8}_{anti}]_2^{6-}$. (Bottom) Using the change in chemical shift of $\mathbf{H}_J$ (ppm) as a function of the overall concentration of $[\mathbf{8}_{anti}]^{3-}$ we obtained stability constant K_a = 510 ± 55 M^{-1} (SigmaPlot) as an arithmetic mean of two separate measurements with the standard deviation as error. A random distribution of residuals is shown at the bottom.

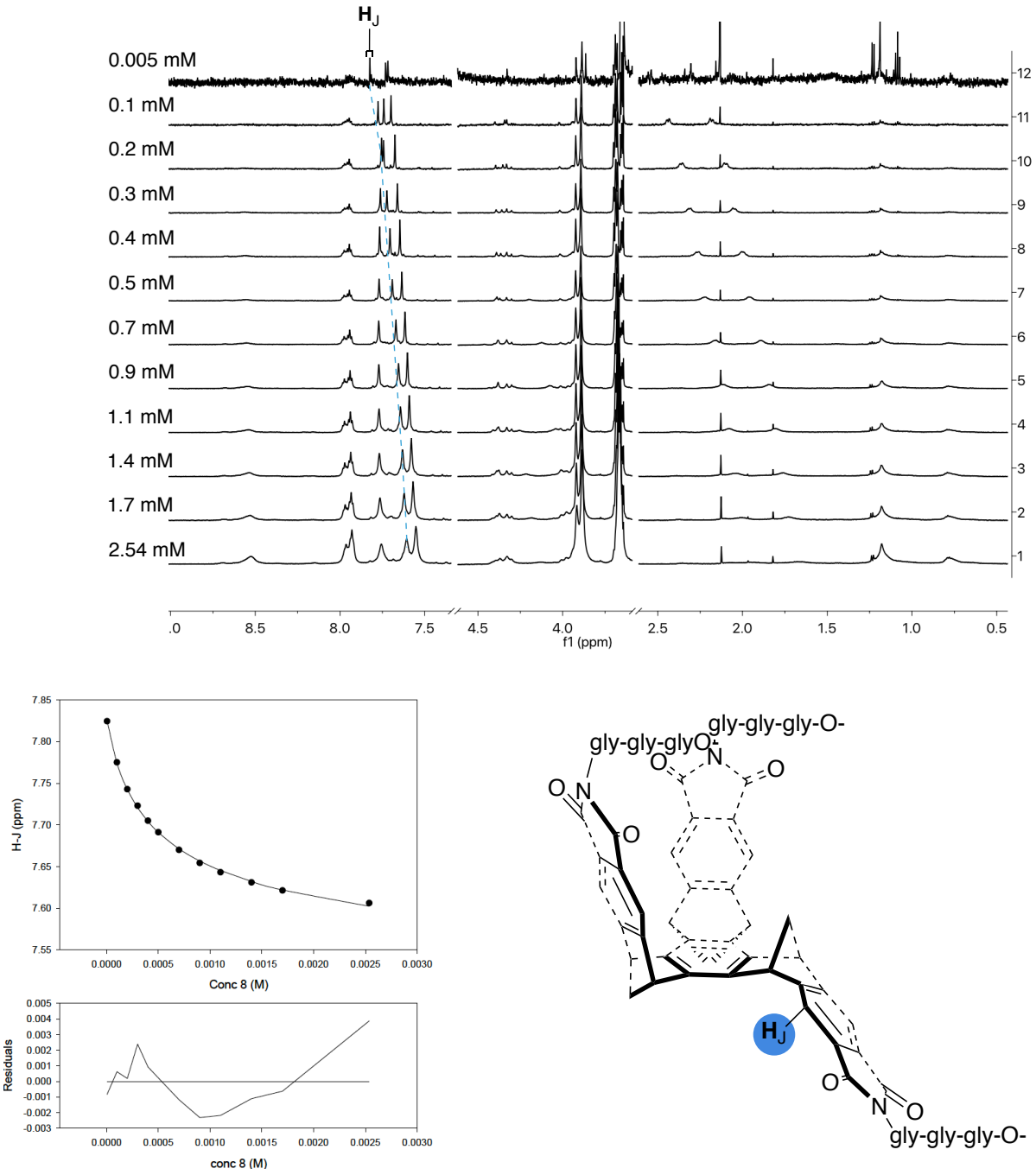

Figure S27. (Top) ^{1}H NMR spectra (600 MHz, 298 K) of $[\mathbf{8}_{anti}]^{3-}$ at different concentrations (shown on the left) in 0.1 M phosphate buffer and containing 0.1 M NaCl at pH = 7.2. (Bottom). Nonlinear least-square analysis of ^{1}H NMR binding data corresponding to the formation of homodimer $[\mathbf{8}_{anti}]_2^{6-}$. (Bottom) Using the change in chemical shift of $\mathbf{H}_J$ (ppm) as a function of the overall concentration of $[\mathbf{8}_{anti}]^{3-}$ we obtained stability constant K_a = 1314 ± 270 M^{-1} (SigmaPlot) as an arithmetic mean of two separate measurements with the standard deviation as error. A random distribution of residuals is shown at the bottom.

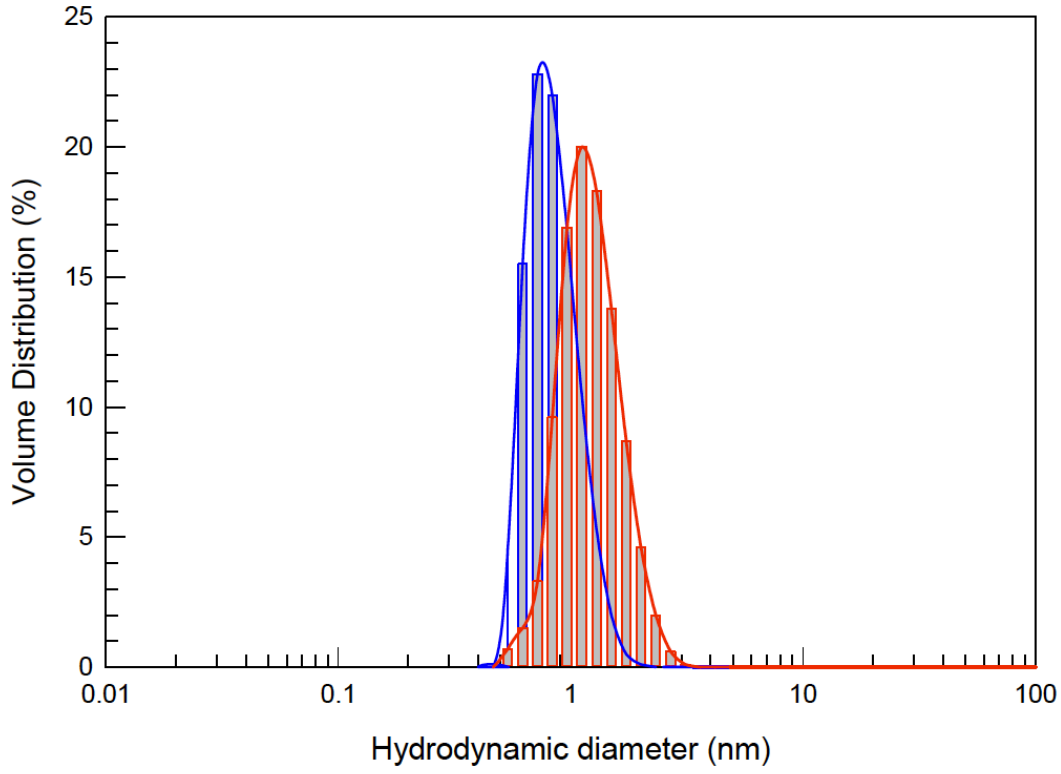

Figure S28. The intensity distributions of scattered light as a function of hydrodynamic diameters (D_H) were obtained from Dynamic Light Scattering (DLS, 298 K) measurements of 0.5 mM (blue, mean count rate = 23-31 kcps, PDI = 0.335-0.621) and 15.0 mM (red, mean count rate = 140-152 kcps, PDI = 0.409-0.503) solutions of $[\mathbf{1}_{anti}]^{3-}$ in 25 mM phosphate buffer at pH = 7.2 ± 0.1; all DLS measurements were completed (in triplicate) on a Malvern Zetasizer Nano Z6 instrument in 25 mM phosphate buffer (pH = 7.2 ± 0.1) that was filtered three times (0.22µm) prior to immediate use. Note that, in the first case (0.5 mM solution), the observed distribution of sizes centers at D_H = 0.8 nm while in the case of more concentrated $[\mathbf{1}_{anti}]^{3-}$ D_H = 1.12 nm therefore indicating the absence of higher oligomers. The observed mean count rates (ideally from 200-500 kbps) are low while the polydispersity indices (PDI) high making the data less reliable yet informative and in line with other measurements.

Computational Studies

Monte-Carlo (MC) conformational searches of $[\mathbf{1}_{anti}]_2^{6-}$, $[\mathbf{2}_{anti}]_2^{6-}$, $[\mathbf{3}_{anti}]_2^{6+}$ and $[\mathbf{2}_{anti}\subset\mathbf{3}_{anti}]$ were each completed with the Maestro suite (Schrodinger) using OPLS3 molecular mechanics (MM) force field in implicit water solvent. For each search, we used systematic torsional sampling method with 100 steps per rotatable bond and 50,000 steps overall. The energy window for saving structures was set to 12 kJ/mol.

For $[\mathbf{1}_{anti}]_2^{6-}$, MC/MM search gave 6 "antiparallel" conformers (0-4.0 kJ/mol, shown on the left) and one parallel homodimer (10.7 kJ/mol, shown on the right). The corresponding steric energies

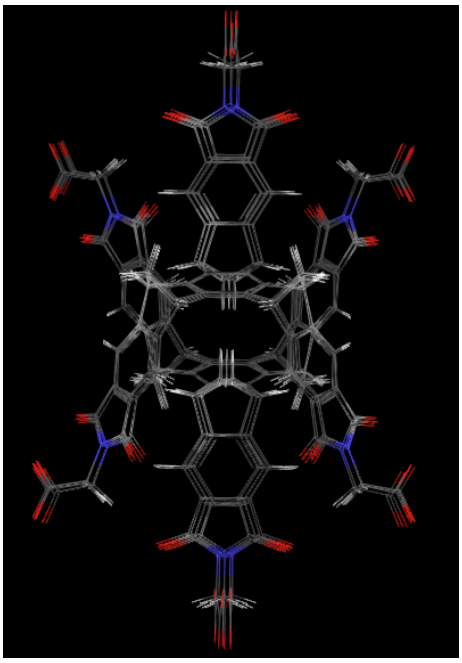

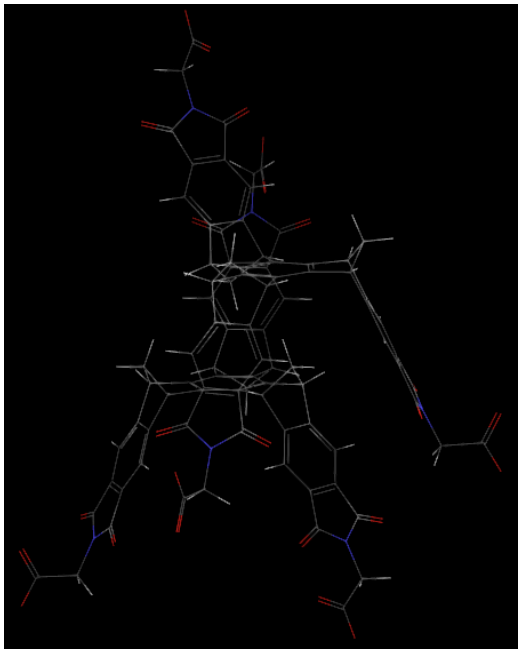

are shown in the table below.

2		Structure1	☆☆☆	2	18 Dec 2…	18 Dec 2018	−1788.743	0.030	0.00
3		Structure1	☆☆☆	3	18 Dec 2…	18 Dec 2018	−1788.743	0.036	0.00
4		Structure1	☆☆☆	4	18 Dec 2…	18 Dec 2018	−1788.336	0.046	0.40
5		Structure1	☆☆☆	5	18 Dec 2…	18 Dec 2018	−1786.572	0.037	2.17
6		Structure1	☆☆☆	6	18 Dec 2…	18 Dec 2018	−1786.569	0.044	2.17
7		Structure1	☆☆☆	7	18 Dec 2…	18 Dec 2018	−1784.681	0.047	4.06
8		Structure1	☆☆☆	8	18 Dec 2…	18 Dec 2018	−1778.029	0.045	10.71

For $[\mathbf{2}_{anti}]_2^{6-}$, MC/MM search gave 3 conformers (0-5.97 kJ/mol, below left) and one (6.36 kJ/mol, below right) populating the equilibrium. The corresponding steric energies are shown in the table below.

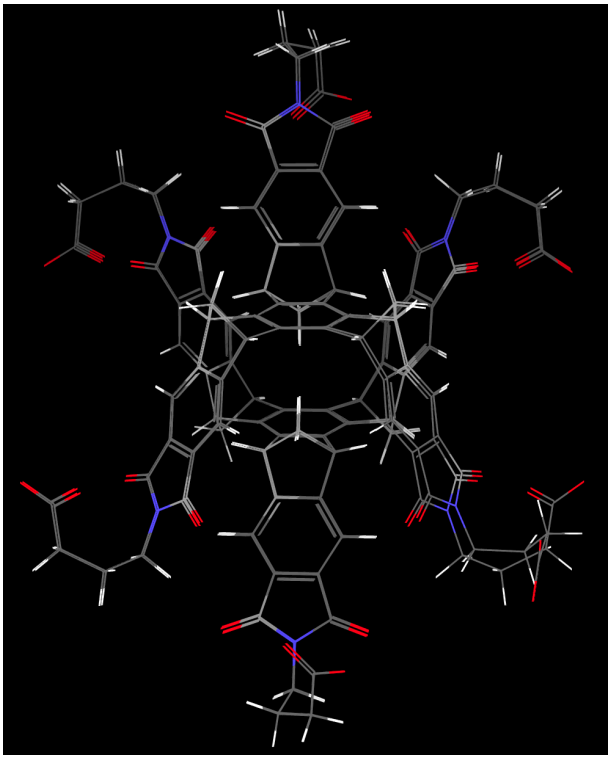

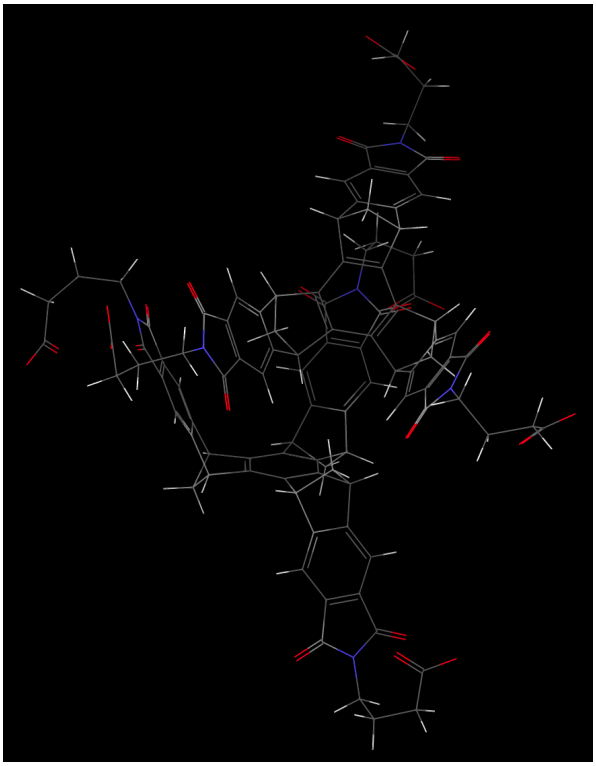

2	Structure1	☆☆☆	2	18 Dec 2…	24 Dec 2018	−1888.810	0.044	0.0
3	Structure1	☆☆☆	3	18 Dec 2…	18 Dec 2018	−1885.553	0.049	3.2
4	Structure1	☆☆☆	5	18 Dec 2…	18 Dec 2018	−1882.448	0.035	6.3
5	Structure1	☆☆☆	4	18 Dec 2…	18 Dec 2018	−1882.842	0.048	5.9
6	Structure1	☆☆☆	6	18 Dec 2…	18 Dec 2018	−1877.208	0.050	11.6

For $[\mathbf{3}_{anti}]_2^{6+}$, MC/MM search gave 31 conformers (0-6.3 kJ/mol, shown below) populating the equilibrium. The corresponding steric energies are shown in the table below.

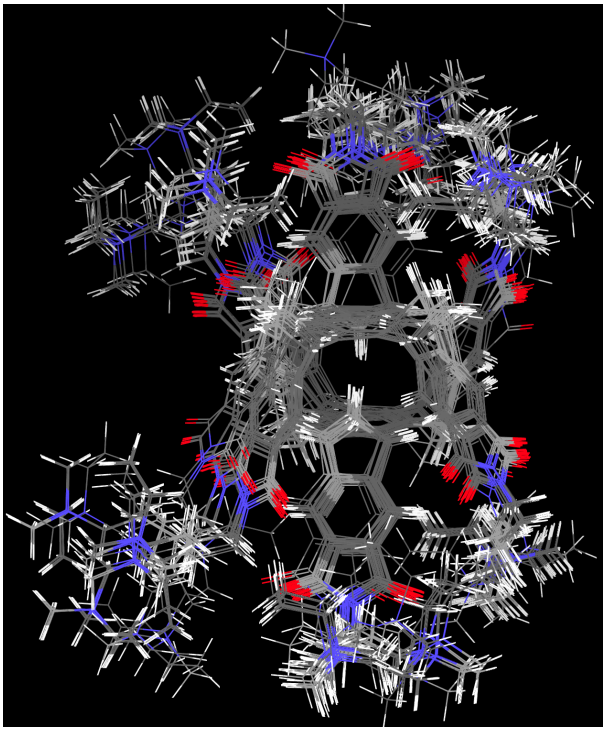

2		Structure1	☆☆☆	2	28 Dec 2…	28 Dec 2018	211.299	0.049	0.000
3		Structure1	☆☆☆	3	28 Dec 2…	28 Dec 2018	211.459	0.049	0.159
4		Structure1	☆☆☆	4	28 Dec 2…	28 Dec 2018	212.626	0.044	1.326
5		Structure1	☆☆☆	5	28 Dec 2…	28 Dec 2018	212.775	0.049	1.476
6		Structure1	☆☆☆	6	28 Dec 2…	28 Dec 2018	213.070	0.037	1.771
7		Structure1	☆☆☆	7	28 Dec 2…	28 Dec 2018	214.065	0.041	2.766
8		Structure1	☆☆☆	8	28 Dec 2…	28 Dec 2018	214.223	0.046	2.924
9		Structure1	☆☆☆	9	28 Dec 2…	28 Dec 2018	214.250	0.048	2.951
10		Structure1	☆☆☆	10	28 Dec 2…	28 Dec 2018	215.090	0.045	3.790
11		Structure1	☆☆☆	11	28 Dec 2…	28 Dec 2018	215.254	0.049	3.955
12		Structure1	☆☆☆	12	28 Dec 2…	28 Dec 2018	215.500	0.049	4.201
13		Structure1	☆☆☆	13	28 Dec 2…	28 Dec 2018	215.513	0.048	4.213
14		Structure1	☆☆☆	14	28 Dec 2…	28 Dec 2018	215.515	0.048	4.216
15		Structure1	☆☆☆	15	28 Dec 2…	28 Dec 2018	215.613	0.043	4.314
16		Structure1	☆☆☆	16	28 Dec 2…	28 Dec 2018	215.673	0.039	4.373
17		Structure1	☆☆☆	17	28 Dec 2…	28 Dec 2018	215.681	0.048	4.382
18		Structure1	☆☆☆	18	28 Dec 2…	28 Dec 2018	216.030	0.044	4.731
19		Structure1	☆☆☆	19	28 Dec 2…	28 Dec 2018	216.110	0.048	4.810
20		Structure1	☆☆☆	20	28 Dec 2…	28 Dec 2018	216.113	0.049	4.814
21		Structure1	☆☆☆	21	28 Dec 2…	28 Dec 2018	216.652	0.048	5.352
22		Structure1	☆☆☆	22	28 Dec 2…	28 Dec 2018	216.770	0.046	5.471
23		Structure1	☆☆☆	23	28 Dec 2…	28 Dec 2018	216.989	0.045	5.690
24		Structure1	☆☆☆	24	28 Dec 2…	28 Dec 2018	217.077	0.049	5.777
25		Structure1	☆☆☆	25	28 Dec 2…	28 Dec 2018	217.081	0.043	5.782
26		Structure1	☆☆☆	26	28 Dec 2…	28 Dec 2018	217.136	0.048	5.836
27		Structure1	☆☆☆	27	28 Dec 2…	28 Dec 2018	217.153	0.049	5.853
28		Structure1	☆☆☆	28	28 Dec 2…	28 Dec 2018	217.216	0.041	5.917
29		Structure1	☆☆☆	29	28 Dec 2…	28 Dec 2018	217.217	0.049	5.918
30		Structure1	☆☆☆	30	28 Dec 2…	28 Dec 2018	217.298	0.045	5.999
31		Structure1	☆☆☆	31	28 Dec 2…	28 Dec 2018	217.426	0.047	6.126
32		Structure1	☆☆☆	32	28 Dec 2…	28 Dec 2018	217.510	0.044	6.210
33		Structure1	☆☆☆	33	28 Dec 2…	28 Dec 2018	217.556	0.045	6.257

For [**2**$_{anti}$⊂**3**$_{anti}$], the MC/MM search gave 61 conformers (0-6.3 kJ/mol, shown below) populating the equilibrium. Steric energies of most stable 30 conformers are shown in the table below.

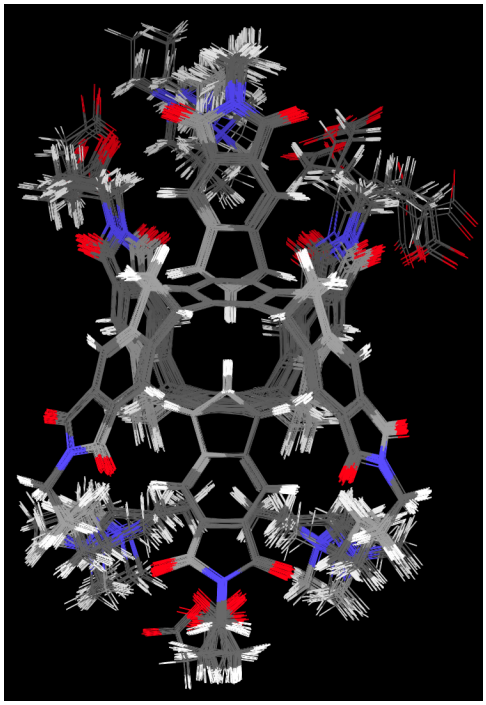

1		Structure1	☆☆☆	1	28 Dec 2…	28 Dec 2018		
	1	mmod_csearch_90-out1 (503)						
2		Structure1	☆☆☆	2	29 Dec 2…	29 Dec 2018	−911.089	0.048	0.000
3		Structure1	☆☆☆	3	29 Dec 2…	29 Dec 2018	−910.220	0.047	0.869
4		Structure1	☆☆☆	4	29 Dec 2…	29 Dec 2018	−909.826	0.045	1.263
5		Structure1	☆☆☆	5	29 Dec 2…	29 Dec 2018	−909.104	0.047	1.985
6		Structure1	☆☆☆	6	29 Dec 2…	29 Dec 2018	−908.366	0.045	2.723
7		Structure1	☆☆☆	7	29 Dec 2…	29 Dec 2018	−908.309	0.050	2.780
8		Structure1	☆☆☆	8	29 Dec 2…	29 Dec 2018	−908.172	0.040	2.917
9		Structure1	☆☆☆	9	29 Dec 2…	29 Dec 2018	−908.030	0.046	3.059
10		Structure1	☆☆☆	10	29 Dec 2…	29 Dec 2018	−907.751	0.043	3.338
11		Structure1	☆☆☆	11	29 Dec 2…	29 Dec 2018	−907.556	0.042	3.533
12		Structure1	☆☆☆	12	29 Dec 2…	29 Dec 2018	−907.508	0.028	3.581
13		Structure1	☆☆☆	13	29 Dec 2…	29 Dec 2018	−907.489	0.049	3.600
14		Structure1	☆☆☆	14	29 Dec 2…	29 Dec 2018	−907.484	0.046	3.605
15		Structure1	☆☆☆	15	29 Dec 2…	29 Dec 2018	−907.330	0.046	3.759
16		Structure1	☆☆☆	16	29 Dec 2…	29 Dec 2018	−907.264	0.045	3.825
17		Structure1	☆☆☆	17	29 Dec 2…	29 Dec 2018	−907.244	0.028	3.845
18		Structure1	☆☆☆	18	29 Dec 2…	29 Dec 2018	−907.113	0.045	3.976
19		Structure1	☆☆☆	19	29 Dec 2…	29 Dec 2018	−907.070	0.042	4.019
20		Structure1	☆☆☆	20	29 Dec 2…	29 Dec 2018	−906.831	0.035	4.258
21		Structure1	☆☆☆	21	29 Dec 2…	29 Dec 2018	−906.754	0.045	4.335
22		Structure1	☆☆☆	22	29 Dec 2…	29 Dec 2018	−906.696	0.050	4.393
23		Structure1	☆☆☆	23	29 Dec 2…	29 Dec 2018	−906.678	0.024	4.411
24		Structure1	☆☆☆	24	29 Dec 2…	29 Dec 2018	−906.595	0.046	4.494
25		Structure1	☆☆☆	25	29 Dec 2…	29 Dec 2018	−906.569	0.048	4.520
26		Structure1	☆☆☆	26	29 Dec 2…	29 Dec 2018	−906.560	0.046	4.529
27		Structure1	☆☆☆	27	29 Dec 2…	29 Dec 2018	−906.436	0.049	4.653
28		Structure1	☆☆☆	28	29 Dec 2…	29 Dec 2018	−906.306	0.042	4.783
29		Structure1	☆☆☆	29	29 Dec 2…	29 Dec 2018	−906.226	0.047	4.863
30		Structure1	☆☆☆	30	29 Dec 2…	29 Dec 2018	−906.133	0.038	4.956
31		Structure1	☆☆☆	31	29 Dec 2…	29 Dec 2018	−906.102	0.046	4.987

Structural optimization of methyl ester of $[\mathbf{1}_{anti}]_2$ was (in vacuum) completed at B3LYP/6-31G* level of theory (DFT) with the Spartan software; the starting structure was obtained from MMFF optimization. Two views of the computed structure of the homodimer are shown below.

```
MacSPARTAN '16 MECHANICS PROGRAM:   (x86/Darwin)                    build  2.0.7

 Frequency Calculation

  Adjusted 35 (out of 576) low frequency modes

  Reason for exit: Successful completion
  Mechanics CPU Time :          1.63
  Mechanics Wall Time:          2.67


MacSPARTAN '16 Quantum Mechanics Program:  (x86/Darwin)     build  2.0.7

Job type: Geometry optimization.
Method: RB3LYP
Basis set: 6-31G(D)
Number of basis functions: 2022
Number of electrons: 876
Parallel Job: 6 threads

SCF model:
 A restricted hybrid HF-DFT SCF calculation will be
 performed using Pulay DIIS + Geometric Direct Minimization


Optimization:
         Step      Energy          Max Grad.      Max Dist.
            1    -5832.001515       0.039331       0.063350
            2    -5832.046258       0.020375       0.063010
            3    -5832.066348       0.013149       0.074110
            4    -5832.074538       0.011015       0.075664
            5    -5832.077092       0.008482       0.075818
            6    -5832.077657       0.005029       0.111500
            7    -5832.078246       0.004004       0.077181
            8    -5832.078680       0.005683       0.043544
            9    -5832.078882       0.005958       0.037149
           10    -5832.078992       0.005116       0.094314
           11    -5832.079107       0.004306       0.082788
           12    -5832.079231       0.005787       0.047738
           13    -5832.079407       0.013498       0.028207
           14    -5832.079504       0.004215       0.047696
           15    -5832.079559       0.003818       0.065315
           16    -5832.079631       0.002654       0.091446
           17    -5832.079708       0.004406       0.089149
           18    -5832.079769       0.003534       0.077581
           19    -5832.079840       0.004088       0.065816
           20    -5832.080010       0.007510       0.085796
           21    -5832.080465       0.017698       0.089469   1
           22    -5832.080902       0.022792       0.071690
           23    -5832.076917       0.185886       0.045344
           24    -5832.081056       0.042878       0.053287
           25    -5832.080671       0.038782       0.117974
           26    -5832.081778       0.008573       0.067847
           27    -5832.081891       0.013246       0.061466
           28    -5832.081969       0.008968       0.058349
           29    -5832.082008       0.006609       0.035567
           30    -5832.082099       0.004333       0.012541
           31    -5832.082101       0.003193       0.011180
           32    -5832.082115       0.002533       0.012936
           33    -5832.082131       0.001420       0.011009
           34    -5832.082138       0.001074       0.008685
           35    -5832.082151       0.000989       0.011258
           36    -5832.082153       0.001797       0.014480
           37    -5832.082179       0.002037       0.019899
           38    -5832.082179       0.001290       0.019843
           39    -5832.082187       0.000713       0.014445
           40    -5832.082178       0.000591       0.013517
           41    -5832.082175       0.000615       0.013440
           42    -5832.082195       0.001158       0.012560
           43    -5832.082205       0.001169       0.014173
           44    -5832.082214       0.000966       0.022511
           45    -5832.082223       0.000928       0.020468
           46    -5832.082223       0.000967       0.065113
           47    -5832.082232       0.001360       0.054659
           48    -5832.082261       0.001929       0.024287
           49    -5832.082272       0.003965       0.015652
           50    -5832.082286       0.001665       0.017290
           51    -5832.082294       0.001233       0.009421
           52    -5832.082307       0.000752       0.037633
           53    -5832.082340       0.000996       0.059234
           54    -5832.082389       0.002088       0.131234   1
           55    -5832.070920       0.101057       0.114089
           56    -5832.082391       0.005647       0.104832
           57    -5832.082431       0.002492       0.080983
           58    -5832.082176       0.014616       0.039336
           59    -5832.082508       0.000624       0.021826
           60    -5832.082518       0.001228       0.011766
           61    -5832.082528       0.001405       0.024226
           62    -5832.082549       0.002425       0.011756
           63    -5832.082550       0.000787       0.047019
           64    -5832.082558       0.002320       0.017555
           65    -5832.082561       0.000628       0.012507
           66    -5832.082566       0.000952       0.024088
           67    -5832.082572       0.000543       0.003721
           68    -5832.082579       0.000550       0.004891
           69    -5832.082579       0.000136       0.002147

  Reason for exit: Successful completion
  Quantum Calculation CPU Time :  79:19:53.24
  Quantum Calculation Wall Time:  15:13:02.91


MacSPARTAN '16 Properties Program:  (x86/Darwin)                build  2.0.7


  Reason for exit: Successful completion
  Properties CPU Time :       3:39.37
  Properties Wall Time:       3:40.85
```

MacSPARTAN '16 MECHANICS PROGRAM: (x86/Darwin) build 2.0.7

Name:	
Formula:	$2C_{48}H_{33}N_3O_{12}$

Job type:	Geometry optimization
Method:	B3LYP
Basis set:	6-31G*
Charge:	neutral
Energy:	-5832.082579 hartrees

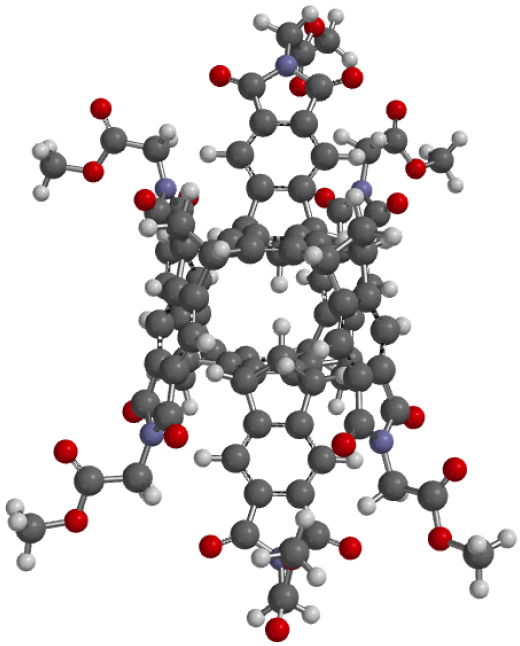

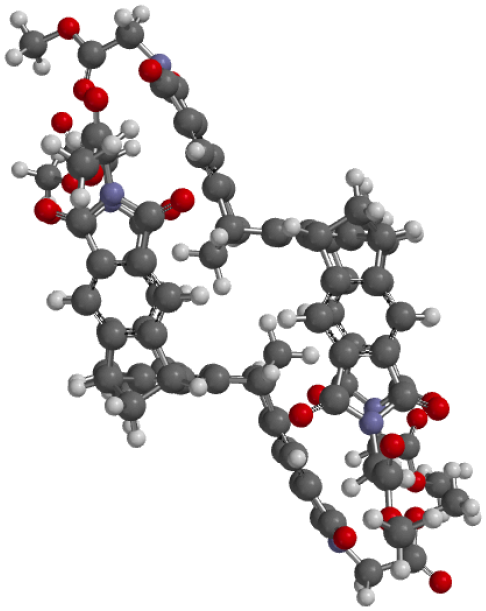

X-Ray Diffraction Data

Note that we used the SQUEEZE program to remove the contribution of a disordered acetonitrile molecule from the structure factor list (see Spek, A. L. (2015). Acta Cryst. C71, 9–18).

Table S1. Crystallographic details for $\mathbf{1}_{anti}$.

Formula	C45 H27 N3 O12 + 6.2 (CH3CN)	
Formula weight	1056.25	
Temperature	150(2) K	
Wavelength	0.71073 Å	
Crystal system	Triclinic	
Space group	P -1	
Unit cell dimensions	a = 8.3179(6) Å	⟨= 93.773(3)°
	b = 17.1721(13) Å	®= 91.789(3)°
	c = 19.0317(14) Å	© = 96.639(3)°
Volume	2692.3(3) $Å^3$	
Z	2	
Density (calculated)	1.303 Mg/m^3	
Absorption coefficient	0.094 mm^{-1}	
F(000)	1100.8	
Crystal size	0.35 x 0.38 x 0.46 mm^3	
Theta range for data collection	2.729 to 25.027°	
Index ranges	-9<=h<=9, -20<=k<=20, -22<=l<=22	
Reflections collected	86712	
Independent reflections	9258 [R(int) = 0.0422]	
Completeness to theta = 25.027°	97.4 %	
Refinement method	Full-matrix least-squares on F^2	
Data / restraints / parameters	9258 / 0 / 710	
Goodness-of-fit on F^2	1.161	
Final R indices [I>2sigma(I)]	R1 = 0.1153, wR2 = 0.3032	
R indices (all data)	R1 = 0.1185, wR2 = 0.3048	
Largest diff. peak and hole	0.685 and -0.533 $e/Å^3$	

Table S2. Hydrogen bonds for $\mathbf{1}_{anti}$ [Å and °].

D-H...A	d(D-H)	d(H...A)	d(D...A)	<(DHA)
C(18)-H(18B)...O(9)#1	0.99	2.33	3.228(8)	151
C(31)-H(31B)...O(2)#2	0.99	2.44	3.414(7)	167
O(4)-H(1O4)...N(1B)	0.94	1.85	2.718(9)	152
O(8)-H(1O8)...N(1D)	1.02	1.81	2.793(9)	161
C(1A)-H(1A3)...O(3)#3	0.98	2.45	3.291(9)	144
C(1D)-H(1D1)...O(2)#4	0.98	2.61	3.235(9)	122
C(1D)-H(1D1)...O(6)#5	0.98	2.42	3.255(9)	142
C(1E)-H(1E2)...N(1F)	0.98	2.35	3.277(15)	158
C(1F)-H(1F1)...O(9)#6	0.98	2.62	3.325(13)	129

Symmetry transformations used to generate equivalent atoms:

#1 x,y-1,z #2 x,y+1,z #3 -x,-y-1,-z+1 #4 -x+2,-y+1,-z+1

#5 -x+2,-y+2,-z+1 #6 -x+1,-y+2,-z